MNRAS **445,** 3496–3511 (2014) doi:10.1093/mnras/stu1944

Pre-main-sequence isochrones – III. The Cluster Collaboration isochrone server

Cameron P. M. Bell,[1,2⋆] Jon M. Rees,[2] Tim Naylor,[2] N. J. Mayne,[2] R. D. Jeffries,[3] Eric E. Mamajek[1] and John Rowe[2]

[1]*Department of Physics & Astronomy, University of Rochester, Rochester, NY 14627-0171, USA*
[2]*School of Physics, University of Exeter, Exeter EX4 4QL, UK*
[3]*Astrophysics Group, Keele University, Staffordshire ST5 5BG, UK*

Accepted 2014 September 17. Received 2014 September 5; in original form 2014 February 12

ABSTRACT

We present an isochrone server for semi-empirical pre-main-sequence model isochrones in the following systems: Johnson–Cousins, Sloan Digital Sky Survey, Two-Micron All-Sky Survey, Isaac Newton Telescope (INT) Wide-Field Camera and INT Photometric Hα Survey (IPHAS)/UV-Excess Survey (UVEX). The server can be accessed via the Cluster Collaboration webpage http://www.astro.ex.ac.uk/people/timn/isochrones/. To achieve this, we have used the observed colours of member stars in young clusters with well-established age, distance and reddening to create fiducial loci in the colour–magnitude diagram. These empirical sequences have been used to quantify the discrepancy between the models and data arising from uncertainties in both the interior and atmospheric models, resulting in tables of semi-empirical bolometric corrections (BCs) in the various photometric systems. The model isochrones made available through the server are based on existing stellar interior models coupled with our newly derived semi-empirical BCs. As part of this analysis, we also present new cluster parameters for both the Pleiades and Praesepe, yielding ages of 135^{+20}_{-11} and 665^{+14}_{-7} Myr as well as distances of 132 ± 2 and 184 ± 2 pc, respectively (statistical uncertainty only).

Key words: techniques: photometric – stars: evolution – stars: formation – stars: fundamental parameters – Hertzsprung–Russell and colour–magnitude diagrams – stars: pre-main-sequence – open clusters and associations: general.

1 INTRODUCTION

1.1 Motivation

Our understanding of the physical processes occurring within stellar interiors has always been driven by the comparison between the outputs predicted by stellar evolutionary models, e.g. masses, luminosities and radii, and the observational data. Open clusters thus provide us with an invaluable testbed with which to assess and constrain these evolutionary models, based in large part on the assumption that the stars within such clusters are of a similar age, distance and chemical composition. Arguably, the most powerful tool for studying clusters is the colour–magnitude diagram (CMD), which provides a robust test of stellar physics as it requires the evolutionary models to work consistently over a broad range of evolutionary states and masses where many different physical processes are acting concurrently. Furthermore, CMDs permit the derivation of age, distance and masses for stellar populations, allowing us to test, for example, whether the initial mass function (IMF) is universal or sensitive to environmental conditions (e.g. Bastian, Covey & Meyer 2010).

In a series of papers, we have investigated the difficulties associated with using pre-main-sequence (pre-MS) model isochrones to derive properties, such as age and mass, from photometric observations of young stars. (Bell et al. 2012, hereafter Paper I) demonstrated that calibrating photometric observations of pre-MS stars using observations of main-sequence (MS) stars can introduce additional significant and systematic uncertainties. In Paper I, we avoided introducing this additional uncertainty by characterizing our adopted natural photometric system. Performing comparisons of the combination of interior and atmospheric models to our observations revealed inherent discrepancies in the optical colours for effective temperatures ($T_{\rm eff}$) $\lesssim 4300$ K. These discrepancies could be as large as a factor of two in the flux at 0.5 μm, resulting in ages derived for young (<10 Myr) stars being underestimated by up to a factor of 3. Paper I was just the latest in a series of papers which have demonstrated that at low masses model isochrones fail to match the

⋆E-mail: cbell@pas.rochester.edu

observed loci of stellar clusters in CMDs (see also Baraffe et al. 1998; Hartmann 2003; VandenBerg & Clem 2003; Bonatto, Bica & Girardi 2004; Pinsonneault et al. 2004; Stauffer et al. 2007). This is also demonstrated in Fig. 5 (see Section 5.2), where the dashed line representing a theoretical isochrone is too blue when compared with photometry of Pleiades members.

Having quantified the discrepancy between the models and the data as a function of $T_{\rm eff}$ in individual photometric bandpasses, (Bell et al. 2013, hereafter Paper II) demonstrated that adopting these empirical corrections resulted in pre-MS model isochrones that matched the observed shape of the pre-MS locus. Using a sample of 13 young clusters, the age of each was assessed from two sets of model isochrones. First, those that follow the nuclear evolution of the relatively massive MS stars, and secondly, those that follow the contraction of low-mass stars to the MS. Adopting our new semi-empirical pre-MS model isochrones, we obtained, for the first time for a set of clusters, consistency between these two age diagnostics for clusters younger than 30 Myr (see also the studies of Lyra et al. 2006; Pecaut, Mamajek & Bubar 2012).

The recent study of NGC 1960 by Jeffries et al. (2013) demonstrates that we are now beginning to establish a reliable age scale for young clusters with ages above 20 Myr from measurements of the lithium depletion boundary (LDB; see also Soderblom et al. 2013), with consistency shown between these ages and those from the MS and pre-MS members of the same cluster. Whilst there is a lower limit to the applicability of the LDB ageing method ($\simeq$20 Myr) due to a higher level of model dependency below this, Paper II highlighted continued consistency between ages derived from MS and pre-MS isochrones down to $\simeq$10 Myr. Thus, we feel the time is now right to make the semi-empirical pre-MS model isochrones we have used to establish this consistency publicly available through an isochrone server.

1.2 Methodology

The use of empirical isochrones to better constrain stellar ages and distances is not unprecedented, and has been applied across a wide range of evolutionary phases including pre-MS (e.g. Stauffer et al. 1998; Jeffries, Thurston & Hambly 2001), older MS (e.g. Pinsonneault et al. 2004; An et al. 2007) and globular clusters (e.g. Brown et al. 2003, 2004). There are several steps involved in creating the semi-empirical pre-MS model isochrones presented in the server, and although these have been detailed in Papers I and II, we feel it is best to reiterate these steps below, in addition to the underlying assumptions which these models are based upon. These steps are summarized in Fig. 1.

In Section 2, we present the photometric systems for which we can create a fiducial locus in CMD space and discuss possible systematic effects on the photometry arising from transformations between different systems. The semi-empirical models rely on us calculating the observed discrepancy between the data and the theoretical model isochrones, and therefore in Section 3 we describe the interior and atmospheric models we have used. In addition to the theoretical model isochrones, we also require parameters for our fiducial clusters (age, distance and reddening) and these are discussed in Section 4.

To calculate quantitatively the mismatch between the data and the models, we need to measure this discrepancy in individual bandpasses. In Paper I, we used a sample of low-mass binaries with well-constrained dynamical masses and multiband photometry to test whether the combination of interior and atmospheric models could reliably predict the combined system magnitudes. This

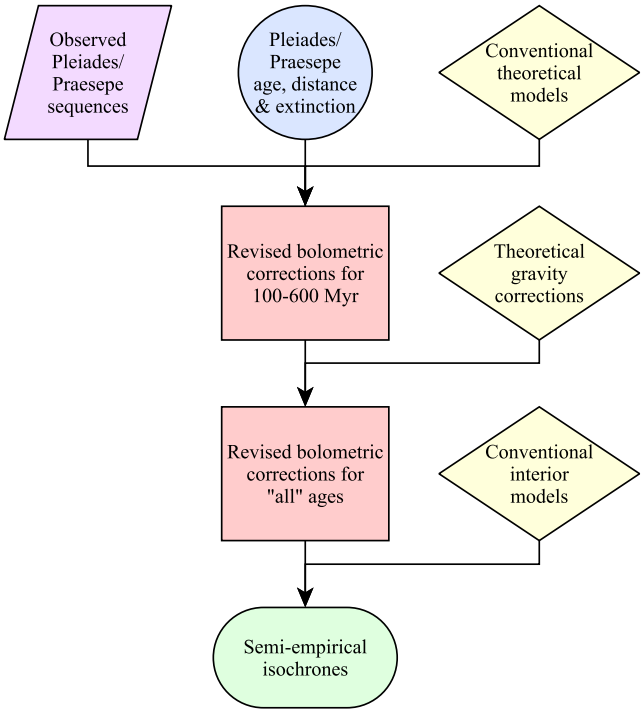

Figure 1. Flowchart summarizing the main steps in creating the semi-empirical pre-MS model isochrones. The purple parallelogram represents the fiducial Pleiades and Praesepe loci, created from observed colours of member stars in each cluster (see Section 2). The blue circle denotes the input age, distance and extinction for the Pleiades and Praesepe (see Section 4). The yellow diamonds signify the theoretical models (both interior and atmospheric; see Section 3). The red rectangles represent the processes of creating the semi-empirical BCs in various photometric systems by comparing the model isochrones to the fiducial loci in CMD space (see Section 5). Finally, the green oval denotes the semi-empirical pre-MS model isochrones which we make available through the server (see Section 7).

showed that whilst the models overpredict the optical fluxes, the predictions for the $K_{\rm s}$ band were essentially correct. We therefore created our colours with respect to the $K_{\rm s}$ band. Hence, assuming that the models reliably predict the relationship between the $K_{\rm s}$ band absolute magnitude and the mass (which appears a reasonable assumption in the mass range covered by our fiducial clusters; see e.g. Delfosse et al. 2000) then this ensures that the resultant semi-empirical model isochrones have a reliable mass scale which is tied to that of the fiducial cluster.

Assumption 1: the theoretical models fit the $K_{\rm s}$-band flux well and therefore we can use this to determine the $T_{\rm eff}$ at points along our fiducial locus and derive the necessary corrections.

Our fiducial locus determines the empirical corrections (here termed ΔBCs) to the theoretical models as a function of $T_{\rm eff}$ for a specific age (or equivalently surface gravity; $\log g$). Thus, if we are to provide semi-empirical model isochrones at different ages, we must assume that the cause of this discrepancy does not depend on $\log g$.

Assumption 2: the empirical corrections in a given bandpass have the same $\log g$ dependence as the theoretical bolometric corrections (BCs). A further assumption concerning the creation of the semi-empirical model isochrones and their application to clusters spanning a wide age range relates to intrinsic differences between clusters of different ages.

Assumption 3: all clusters are assumed to behave like the Pleiades such that there are no intracluster effects due to, for example, binary fractions and mass ratios, intrinsic age spread, rotation distribution and activity-related effects on the observed colours.

Section 5 describes the process of quantifying this discrepancy between the uncorrected models and the data in more detail. For reasons discussed in Paper I, we choose the Pleiades as our default fiducial cluster for all photometric systems discussed here. For the Sloan Digital Sky Survey (SDSS) system, however, there are no Pleiades data and so in Section 6, we discuss what effect adopting a different cluster (Praesepe) has on our semi-empirical model isochrones.

Our isochrone server is introduced in Section 7 and we give a brief overview of its use. Our primary aim in making these model isochrones available is to allow others to measure cluster ages from the pre-MS which are consistent with those we have derived. In addition, these models can also be used to identify possible new cluster members from their positions in CMDs which would then require spectroscopic follow-up. Finally, these models could also be used to calculate mass functions for stellar populations based on their positions in the CMD. We advise users that given the processes involved in creating these model isochrones, they should *not* be used to compare against new cluster photometry and then argue that, due to a mismatch between the models and the data, there is a particular problem with either the interior or atmospheric models.

2 THE DATA

In this section, we discuss the photometric systems for which we are able to construct a well-populated fiducial locus in CMD space using data from a young cluster with known age and distance. Here, we only discuss the data and memberships adopted, whilst in Section 4, we discuss the adopted fiducial cluster parameters and in Section 5.1, we describe the process of creating the single-star locus. In this paper, we will focus on five photometric systems: Johnson-Cousins, Isaac Newton Telescope Wide-Field Camera (INT-WFC), INT Photometric Hα Survey (IPHAS)/UV-Excess Survey (UVEX), Two-Micron All-Sky Survey (2MASS) and SDSS.

2.1 Johnson–Cousins

Our starting point for a Pleiades catalogue in the Johnson–Cousins photometric system is the $BVI_{\rm c}$ catalogue of Stauffer et al. (2007). The membership catalogue of Stauffer et al. represents a number of photometric, photoelectric and photographic surveys which have been combined with a series of proper motion surveys to assign cluster membership. The reader is directed to Appendix A1 of Stauffer et al. (2007) for a full and comprehensive discussion of the catalogues used.

To include R band photometry, we adopted Johnson $(R-I)_{\rm J}$ measurements for stars brighter than $V \simeq 11$ from Mendoza (1967). These Johnson colour indices were converted to Cousins indices using the following relation from Bessell (1979):

$$(R-I)_{\rm c} = 0.856(R-I)_{\rm J} + 0.025 + \Delta(R-I)_{\rm J}, \quad (1)$$

where $\Delta(R-I)_{\rm J}$ is a non-linear correction curve and for which the transformation is accurate to within 0.02 mag for MS stars with colours $(R-I)_{\rm c} \lesssim 0.7$. For stars fainter than $V \simeq 11$, we used the photometric data from Stauffer (1980, 1982, 1984) and Stauffer & Hartmann (1987). These studies present $(RI)_{\rm K}$ photometry in the Kron system and so these too were transformed into Cousins colour indices using a relation from Bessell & Weis (1987):

$$(R-I)_{\rm c} = 0.102 + 0.9166(R-I)_{\rm K} + 0.4230(R-I)^2_{\rm K} - 0.16647(R-I)^3_{\rm K}, \quad (2)$$

which is accurate to within 0.02 mag for MS stars with colours $(R-I)_{\rm c} \lesssim 2.2$. Additional Cousins $(RI)_{\rm c}$ photometry for very low-mass stars and brown dwarfs was taken from Bouvier et al. (1998); however, we only retained confirmed proper motion members as defined in Moraux, Bouvier & Stauffer (2001).

At the age of the Pleiades the majority of stars have reached the MS; however, those with masses below $\sim$0.4 $M_{\odot}$ are still undergoing pre-MS contraction. In Paper I, we discussed the problems with using MS relations to transform photometric observations of pre-MS stars which stem from a combination of differences in $\log g$ as well as in the spectra between MS and pre-MS stars of the same colour. Hence, what effect does using MS relations to transform the Kron $(RI)_{\rm K}$ photometry of the low-mass pre-MS members have on our fiducial sequence in the Cousins $(RI)_{\rm c}$ colours?

Using the Dotter et al. (2008) and updated Pisa evolutionary models (see Section 3.1), we estimate that the difference in $\log g$ between a 0.1 $M_{\odot}$ star (approximately the lowest mass in the Kron photometric sample) at an age of 130 Myr and its arrival on the ZAMS ($\sim$20 Gyr; Siess, Dufour & Forestini 2000) is $\sim$0.2–0.3 dex. Assuming this difference in $\log g$, we can roughly quantify the possible systematic uncertainty introduced into the transformed photometry using the derived $(RI)_{\rm c}$ BCs (see Section 3.2). From these, we estimate that the uncertainty in the $(R-I)_{\rm c}$ colour as a result of the differences in the $\log g$ between a pre-MS and ZAMS star of mass $\simeq$0.1 $M_{\odot}$ is $\leq$0.05 mag (allowing for slight variations in $T_{\rm eff}$ depending on which evolutionary model is adopted). Contrast this with a difference of $\simeq$0.1–0.15 mag at an age of 3 Myr.

Such a systematic uncertainty is not ideal; however, given that our choice of populated fiducial clusters is so limited, coupled with the fact that the Cousins $(RI)_{\rm c}$ bandpasses have surpassed the Kron $(RI)_{\rm K}$ bandpasses as the de facto choice of optical RI bandpasses, there is little option but to proceed with the transformed photometry. We note, however, that we are correcting for an observed discrepancy of $\simeq$0.3 mag, and that after having done so, the recalibrated model isochrones have a residual systematic uncertainty at the 0.05 mag level in $(R-I)_{\rm c}$. Furthermore, it is worth noting that the $V-I_{\rm c}$ colours given in the Stauffer et al. (2007) catalogue represent values transformed using a relation from Bessell & Weis (1987) based on the same MS sample as those used to derive equation (2); however, no discussion of introduced systematic uncertainties is given in the paper.

2.2 Isaac Newton Telescope Wide-Field Camera

The Pleiades data in the natural photometric system of the INT-WFC is that described in Papers I and II. As the photometric observations presented in these studies extend to lower masses than the Johnson–Cousins sequence it was necessary to supplement the Stauffer et al. (2007) membership catalogue with lower mass members from Lodieu, Deacon & Hambly (2012, see Paper I for a discussion).

A large benefit of including the INT-WFC in this study is due to the WFC's use in both IPHAS (Drew et al. 2005) and UVEX (Groot et al. 2009). These combined surveys use a combination of the $(Ugri)_{\rm WFC}$ and narrow-band $H\alpha$ bandpasses to survey a sky area of approximately 1800 deg^2 in the northern Galactic plane spanning the latitude range $-5^{\circ} < b < +5^{\circ}$ to a limit $r_{\rm WFC} \simeq 20$.

Table 1. The bandpass specific zero-point shifts required to convert magnitudes in the INT-WFC (AB) photometric system to the IPHAS/UVEX (Vega) system.

Bandpass	INT-WFC – IPHAS/UVEX
$g_{\rm WFC}$	−0.090
$r_{\rm WFC}$	+0.147
$i_{\rm WFC}$	+0.394

Unfortunately, we do not have useful $U_{\rm WFC}$-band photometry nor $H\alpha$ observations of the Pleiades and hence these bandpasses are not included in the following discussion.

Whilst our own observations are calibrated to an AB magnitude system to replicate the SDSS (at least approximately), the IPHAS and UVEX surveys are calibrated on to a Vega system. To distinguish between these two systems, we will refer to the IPHAS/UVEX system in addition to our own INT-WFC system. The difference between the two is a simple zero-point offset, which is given in Table 1, calculated by folding the reference spectrum of Vega and the AB zero-point flux distributions (see Section 3.2) through the system responses given in Paper I. The differences between these and the values given in Table 1 of González-Solares et al. (2008) are likely attributable to small differences in the adopted responses.

2.3 Two-Micron All-Sky Survey

The 2MASS (Skrutskie et al. 2006) data cover an area of $2^\circ \times 3^\circ$ centred on the Pleiades cluster and represent a subset of the so-called 6×observations[1] (see Cutri et al. 2012). These observations were taken towards the end of the 2MASS survey with exposures six times longer than those used for the primary survey. We have adopted the members defined in Stauffer et al. (2007), for which memberships have been assigned in an identical fashion to those described in Section 2.1.

2.4 Sloan Digital Sky Survey

The Pleiades cluster was not observed as part of the SDSS (York et al. 2000) and therefore we require an alternative cluster. Cross-correlating the positions of the Dias et al. (2002) open cluster catalogue with the Ninth Data Release of the SDSS (Ahn et al. 2012), we find only two other suitable cluster candidates, namely IC 4665 and Praesepe. Unfortunately, although IC 4665 has an LDB age, the sequence in CMD space (defined using the Jeffries et al. 2009 members) is extremely sparse and does not provide a well-sampled population of stars across a significant colour range. Praesepe, therefore, offers an appealing alternative on the basis of the following: (i) it is a rich cluster, (ii) it is nearby, thereby allowing us to access the lowest mass members, (iii) it has a very low uniform reddening and (iv) it has a well-defined sequence in the CMD.

We used the Praesepe members as defined by Kraus & Hillenbrand (2007) with membership probabilities of ≥95 per cent. Using this refined membership list, we selected SDSS photometry for each source by requiring that: (i) the object is classified as a star ('Type'=6), (ii) the uncertainty on the magnitude in each bandpass is ≤0.1 mag and (iii) the photometry flags 'BLENDED' (whether the object is a composite), 'EDGE' (whether the object was too close to the edge of the frame) and 'SATURATED' (whether the object contains any saturated pixels) are all false in each bandpass.

Note that there are two specific issues which need to be addressed when adopting Praesepe as our alternative fiducial cluster. First, there is the issue of increased magnetic activity at younger ages (see e.g. Stauffer et al. 2003) and what effect this may have on the observed colours of stars (in relation to those in the Pleiades). Secondly, there is the matter of metallicity and the possible systematic residuals introduced by using a non-solar composition locus to recalibrate solar metallicity pre-MS model isochrones. In Section 6, we provide a detailed discussion of both of these issues and demonstrate that, when compared to the observed discrepancy between the models and the data, these effects are not significant.

3 THE MODELS

Before we can quantify the discrepancy between the theoretical model isochrones and the observed colours of the fiducial loci in CMD space, we must first create the model isochrones using a combination of interior and atmospheric models. The atmospheric models are used to convert the bolometric luminosities ($L_{\rm bol}$), $T_{\rm eff}$ and $\log g$ predicted by the interior models into observable colours and magnitudes. This conversion is based on BC–$T_{\rm eff}$ relations, which can be derived by folding the flux distribution of theoretical atmospheric models through the appropriate photometric system responses. Here, we describe the stellar interior and atmospheric models used in this paper.

3.1 Stellar interior models

In addition to the pre-MS model isochrones which we make available via the isochrone server, we also require MS models to derive the cluster parameters for Praesepe and ensure that these are consistent with those we have adopted for the Pleiades. To ensure consistency with the MS ages we have derived in Paper II, we adopt the same resampled grid of Lejeune & Schaerer (2001), specifically the basic 'c' grid (Schaller et al. 1992), with spacing $\Delta\log(\text{age}) = 0.02$. In the pre-MS regime, we used the Baraffe et al. (1998) with a solar-calibrated mixing-length parameter $\alpha = 1.9$ and the Dotter et al. (2008) models (hereafter BCAH98 $\alpha = 1.9$ and DCJ08, respectively).

The semi-empirical pre-MS model isochrones created in this paper and distributed via the server comprise of semi-empirical BCs coupled with existing pre-MS interior models. The interior models we choose to adopt for the server consist of the BCAH98 $\alpha = 1.9$, DCJ08 and Pisa groups (Tognelli, Prada Moroni & Degl'Innocenti 2011). In Paper I, we were unable to test these models as they did not extend to the age of the Pleiades; however, Emanuele Tognelli has kindly computed an updated set of Pisa models spanning a mass range 0.08−9 $M_\odot$ and extending to ages of ∼10 Gyr at 1 $M_\odot$ (private communication). To ensure that the updated Pisa models predict ages that are consistent with the ages derived from the higher mass MS stars, we have used the τ^2 fitting statistic (see Naylor & Jeffries 2006) to calculate pre-MS ages for the five young clusters we previously fitted in Paper II; namely λ Ori, NGC 2169, NGC 2362, NGC 7160 and NGC 1960. We find that the ages derived using the updated Pisa models agree with those calculated using the DCJ08 models to within ±1 Myr, and are therefore generally consistent with the MS ages for the regions as calculated in Paper II.

[1] A general overview as well as additional information concerning the 6×observations, data reduction and catalogue can be found at http://www.ipac.caltech.edu/2mass/releases/allsky/doc/seca3_1.html

Table 2. Photometric systems (and the individual bandpasses) adopted in this paper. The reference directs the reader to the source for the system responses adopted for each system.

Photometric system	System responses	Reference
Johnson–Cousins	$BV(RI)_c$	Bessell & Murphy (2012)
INT-WFC	$(griZ)_{WFC}$	Paper I
SDSS	$griz$	Doi et al. (2010)
2MASS	JHK_s	Cohen et al. (2003)

The basic input assumptions concerning the stellar interior structure and physics are the same as those described in Tognelli et al. (2011); however, we describe some recent updates. The standard Pisa models adopted the equation of state (EOS) of Rogers & Nayfonov (2002) to the limiting mass of 0.2 $M_\odot$. The updated models, however, extend to much lower masses and so for masses below 0.2 $M_\odot$ they are computed using the EOS of Saumon, Chabrier & van Horn (1995). For the outer boundary conditions, the BT-Settl atmospheric models of Allard, Homeier & Freytag (2011) were used for $T_{\rm eff} < 2000$ K, the PHOENIX/*GAIA* models of Brott & Hauschildt (2005) for $2000 \leq T_{\rm eff} < 10\,000$ K, and the ATLAS9/ODFnew models of Castelli & Kurucz (2004) for $T_{\rm eff} \geq 10\,000$ K. The models use the OPAL EOS 2005 radiative opacity table (see e.g. Iglesias & Rogers 1996) for $\log T_{\rm eff} \geq 4.5$, and for cooler temperatures that of Ferguson et al. (2005). Note that both opacity tables have been computed using the more recent Asplund et al. (2009) heavy element solar abundances. The mixing length parameter α has been tuned to fit the observed properties of the present day Sun and is calculated to be $\alpha = 1.74$. The updated interior models also include the effects of convective core overshooting – the quantity which characterizes the distance that convective elements penetrate beyond the classical core in terms of pressure scaleheights – which has been set to $\lambda_{\rm over} = 0.2$ for masses greater than 1.1 $M_\odot$ (see Tognelli, Degl'Innocenti & Prada Moroni 2012).

3.2 Atmospheric models

The atmospheric models used are the same as those in Papers I and II. For $T_{\rm eff} < 8000$ K, we adopt the PHOENIX BT-Settl models (Allard et al. 2011), whereas for $8000 \leq T_{\rm eff} \leq 50\,000$ K, we use the Kurucz ATLAS9/ODFnew models (Castelli & Kurucz 2004).

We derive BCs for the Johnson–Cousins, INT-WFC, 2MASS and SDSS photometric systems using equation (B2) in Appendix B of Paper I for which we adopt the system responses of Bessell & Murphy (2012), Paper I, Cohen, Wheaton & Megeath (2003) and Doi et al. (2010), respectively (see Table 2). To calculate BCs for each photometric system, we require a reference spectrum which produces a known magnitude in a given bandpass. For the Johnson–Cousins BCs, we used the CALSPEC Vega reference spectrum alpha_lyr_stis_005[2] with $V = 0.03$ and all colours equal to zero. In the 2MASS photometric system, we used the bandpass specific reference spectra and the zero-point offsets of Cohen et al. (2003). Finally, for the INT-WFC and SDSS systems, we used a reference spectrum of constant flux density per unit frequency f_ν° (see e.g. Oke & Gunn 1983) converted into energy per unit wavelength according to $f_\lambda = c/\lambda^2 f_\nu$ which results in reference magnitudes of zero in all bandpasses. In addition to the reference spectra, we also require solar values for the absolute bolometric magnitude and luminosity for which we adopt $M_{\rm bol,\odot} = 4.755$ mag and $L_\odot = 3.827 \times 10^{33}$ erg s^{-1} as given in Mamajek (2012).

[2] http://www.stsci.edu/hst/observatory/cdbs/calspec.html

4 THE AGE AND DISTANCE OF OUR FIDUCIAL CLUSTERS

To use the empirical colours of the fiducial loci in CMD space to quantify the discrepancy between the theoretical models and the observed data, we must first adopt a set of parameters (age, distance and reddening) representative of the cluster and apply these to the theoretical model isochrones.

4.1 The Pleiades

In the case of the Pleiades, we adopt (as in Paper I) a distance modulus $dm = 5.63$ mag derived via space-based trigonometric parallax measurements (Soderblom et al. 2005), an age of 130 Myr based on detecting the LDB in the K_s band (Barrado y Navascués, Stauffer & Jayawardhana 2004), and a reddening of $E(B-V) = 0.04$ mag (Stauffer et al. 1998).[3]

4.2 Praesepe

Praesepe is a much more evolved cluster and therefore we are unable to make use of the LDB to calculate an age. In addition, although the revised *Hipparcos* distance modulus of $dm = 6.30$ mag (van Leeuwen 2009) is in good agreement with other determinations (e.g. An et al. 2007), the uncertainty in this distance modulus (almost 0.1 mag) is too large for the purposes of calculating empirical BCs at low $T_{\rm eff}$. Hence, we derive a consistent age and distance for Praesepe from fitting photometry of MS members in the $V, B-V$ CMD using MS evolutionary models.

Age and distance estimates will be affected by both reddening and metallicity. As Praesepe is significantly older than the Pleiades, the higher mass members have already evolved off the MS and entered the post-MS evolutionary phase. Hence, we are unable to derive a reddening using these members in the $U-B, B-V$ colour–colour diagram (see e.g. Mayne & Naylor 2008). Instead, we adopt the mean value of $E(B-V) = 0.027$ mag derived using a combination of polarization measurements, comparison of β and $(R-I)_c$ for F stars, and Strömgren β analysis of A stars (Taylor 2006).

An additional consideration is the chemical composition of Praesepe. Relative to the composition of the Pleiades, which to within the uncertainties is solar ([Fe/H] $= +0.03 \pm 0.02 \pm 0.05$ dex [statistical and systematic]; see Soderblom et al. 2009), the metallicity of Praesepe is supersolar. Literature values for the absolute difference between the metallicity of the Pleiades and Praesepe vary from Δ[Fe/H] $= 0.07 - 0.09$ dex (see An et al. 2007; Boesgaard,

[3] We independently estimate the reddening to the Pleiades through two methods. First, using the Q-method of Johnson & Morgan (1953) with the homogenized photometry of 15 B-type Pleiades members from Mermilliod (2006), in conjunction with the revised $Q/U-B/B-V$ sequences of Pecaut & Mamajek (2013), we estimate a mean reddening of $E(B-V) = 0.036 \pm 0.006$ mag. Secondly, using the *ubvy* photometry of 15 B-type Pleiades members from Hauck & Mermilliod (1998) and dereddening following Castelli (1991), and the $E(b-y)/E(B-V)$ slope from Taylor, Joner & Jeffery (2008), we estimate a mean reddening of $E(B-V) = 0.044 \pm 0.005$ mag. Both of these estimates are in agreement with the value of $E(B-V) = 0.04$ mag we have adopted from Stauffer et al. (1998).

Roper & Lum 2013 respectively). We therefore adopt the mean value (0.08 dex) which translates to $Z_{\rm Praesepe} = 1.2\,Z_{\rm Pleiades}$.

We performed a quadratic interpolation for both the interior and atmospheric models to produce grids of each with a metallicity equal to $1.2\,{\rm Z}_{\odot}$. We note that at this metallicity, the choice of interpolation scheme does not significantly affect the derived best-fitting values for the age and distance, i.e. adopting a linear interpolation we find that the values of parameters are only affected at the $\sim 1\sigma$ level. To transform the theoretical models into CMD space, we reddened the atmospheric models by a nominal $E(B-V) = 0.027$ mag using the Galactic reddening law of Fitzpatrick (1999) with $R_V = 3.1$ and then calculated the BCs as described in Section 3.2 using the Bessell & Murphy (2012) system responses.

We used the τ^2 fitting statistic (Naylor & Jeffries 2006; Naylor 2009) to fit the MS evolutionary models to the *UBV* photometric data of Praesepe from Johnson (1952). The reader is referred to Paper II for a complete description of this process including the creation of the two-dimensional distributions and how we include the effects of binaries in the simulated population. The only difference is that as opposed to the power-law distribution adopted in Paper II, which results in a roughly even distribution of stars as a function of magnitude, we instead opt for the canonical broken power-law IMF presented in Dabringhausen, Hilker & Kroupa (2008). Even though we have adopted a different mass function for this study, we note that the choice of mass function does not have a significant impact on the derived best-fitting parameters (see Naylor 2009) and hence the MS parameters we derive here are on a consistent scale with the MS parameters we have derived in Paper II. If the assigned secondary mass is less than the lower mass limit of the interior models (which in the case of the Schaller et al. 1992 models is $0.8\,{\rm M}_{\odot}$), we begin to lose the binary population before the single-star sequence in our two-dimensional distribution, resulting in a 'binary wedge' (see Jeffries et al. 2007). To avoid this affecting our fitting of the photometric data, we combine the Schaller et al. (1992) models with those of Dotter et al. (2008), which extend to masses of $0.1\,{\rm M}_{\odot}$. Between 1 and $0.8\,{\rm M}_{\odot}$ the two models show excellent agreement, and so we use the Schaller et al. (1992) models down to $1\,{\rm M}_{\odot}$ and append the Dotter et al. (2008) models from 1 to $0.1\,{\rm M}_{\odot}$.

The best-fitting $V, B-V$ CMD for Praesepe is shown in Fig. 2. Prior to fitting, we removed four stars defined as giants in Johnson (1952) in addition to one star which appears to have evolved off the MS as these would impact our derived values. Furthermore, we removed four additional stars due to a combination of their positions in the $V, B-V$ CMD and their associated τ^2 values which lie blueward of the MS locus. From the remaining stars, we derive an age of 665^{+14}_{-7} Myr and a distance modulus $dm = 6.32 \pm 0.02$ mag with an associated $\Pr(\tau^2) = 0.87$ (statistical uncertainties only). As noted in Paper II, the Schaller et al. (1992) models do not include the pre-MS evolutionary phase, but only that from the ZAMS onwards. The age we derive for Praesepe is driven by the most massive stars, i.e. those have evolved significantly away from the ZAMS. These most massive stars in Praesepe typically have spectral types of ~A5 (see e.g. Bidelman 1956), which, from the evolutionary models of Siess et al. (2000), take ~5 Myr to reach the ZAMS. Hence, although the Schaller et al. (1992) models do not include the pre-MS evolutionary phase, the time-scale involved is shorter than the uncertainties on the derived age and can therefore be ignored.

The values that we have derived for the age and distance to Praesepe are consistent with, yet more precise than, previous estimates e.g. 700 ± 100 Myr (Salaris, Weiss & Percival 2004), 590^{+150}_{-120} Myr (Fossati et al. 2008) and $dm = 6.30 \pm 0.07$ (van Leeuwen 2009). We note, however, that our derived age is significantly younger than that of Gáspár et al. (2009), who find an age of 757 ± 36 Myr via isochrone fitting. Gáspár et al. (2009) use SDSS photometry; however, for bright stars the photometric measurements can be unreliable due to saturation effects. They therefore replace some of these measurements with transformed Johnson *BV* data; however, only when the difference between the transformed value and the original SDSS measurement is greater than 0.5 mag. Thus, compared to the level of calibration and consistency in the Johnson *BV* photometry we have used here, it is plausible that the age discrepancy could be due to residual unreliable photometry in the Gáspár et al. (2009) sample.

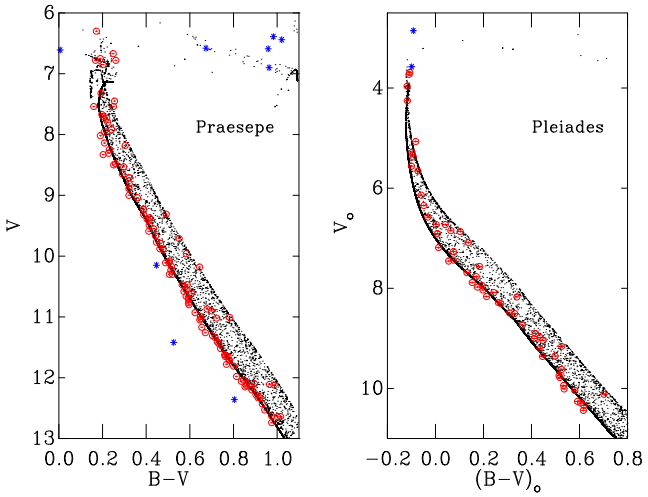

Figure 2. Best-fitting CMDs of Praesepe and the Pleiades. Left: the best-fitting $V, B-V$ CMD for Praesepe with a derived age of 665 Myr and distance modulus $dm = 6.32$ mag. Circles represent the data of Johnson (1952), with the associated uncertainties shown as the bars. Asterisks represent stars that were clipped before deriving the best fit (see text). Right: the best-fitting de-reddened $V_\circ, (B-V)_\circ$ CMD for the Pleiades with an age of 135 Myr and distance modulus $dm = 5.61$ mag. The data and uncertainties are from Johnson & Morgan (1953).

We were concerned that different techniques had been used to derive the ages and distances for Praesepe and the Pleiades, which may be systematically different. As a check we therefore determined the Pleiades parameters using the same technique we had used for Praesepe. Starting with the photometric data of Johnson & Morgan (1953), we de-reddened the stars blueward of $B-V = 0.0$ on a star-by-star basis using the revised Q-method (see Mayne & Naylor 2008, Paper II) as there was evidence of spatially variable extinction in the $U-B, B-V$ colour–colour diagram. Stars redward of $B-V = 0.0$ were de-reddened using the same reddening vectors assuming a median reddening of $E(B-V) = 0.03$ mag (as calculated from the bluer stars). We fitted the entire data set, deriving an age of 135^{+20}_{-11} Myr and distance modulus $dm = 5.61^{+0.03}_{-0.02}$ mag with an associated $\Pr(\tau^2) = 0.23$ (see Fig. 2, cf. 130 Myr and $dm = 5.63$). Note that to achieve this fit it was necessary to remove the two brightest stars from our sample. The reason for this may simply be that we do not have enough stars in our simulated distribution to get enough density in that region of the CMD. Regardless, we can be reasonably confident that although we are using a different fiducial locus in the SDSS photometric system, the adopted parameters for both fiducial clusters are on a consistent age and distance scale.

5 CREATING SEMI-EMPIRICAL PRE-MS ISOCHRONES

The problems associated with using pre-MS model isochrones to derive ages and masses from photometric data have been well documented over the past two decades. It is strongly believed that such problems stem from underlying uncertainties in both the stellar interior and atmospheric models, especially at younger ages and lower $T_{\rm eff}$ (e.g. Stauffer et al. 1998; Baraffe et al. 2002; Hillenbrand & White 2004; Mayne et al. 2007; Da Rio et al. 2010a). In Paper I, we demonstrated that there are severe problems with using atmospheric models to transform pre-MS evolutionary models into CMD space, where for $T_{\rm eff} \lesssim 4300$ K the *combined* models overestimate the flux in the optical by up to a factor of 2. Hence, if we are to use pre-MS model isochrones to derive consistent ages and masses for young stellar populations using CMDs, it is clear that we must adopt empirical BCs for $T_{\rm eff}$ lower than $\simeq$4300 K.

5.1 Deriving semi-empirical BC–$T_{\rm eff}$ relations

To define the locus in each of the photometric systems, we fitted a spline (by eye) to the single-star sequence of the Pleiades for the Johnson–Cousins, 2MASS, INT-WFC and systems and Praesepe for the SDSS. To determine the position of the spline in CMD space, we only used stars with uncertainties in both colour and magnitude of $\leq$0.1 mag. The splines are fitted as described in Paper I and positioned taking into account the fact that the equal-mass binary locus lies $\simeq$0.75 mag above the single-star locus (with very few systems of higher multiplicity). The single-star sequence for the Pleiades in the combined Johnson–Cousins, 2MASS and INT-WFC bandpasses is given in Table 3, whereas the Praesepe sequence in the SDSS bandpasses is given in Table 4. The Pleiades single-star sequence in the IPHAS/UVEX system can be created by adopting the magnitudes in the INT-WFC bandpasses from Table 3 and converting these according to the transformations given in Table 1.

We have made a small modification to the single-star sequence in the $K_{\rm s}, g_{\rm WFC} - K_{\rm s}$ CMD (in comparison to that given in Paper I) in the colour range where we suffered from a paucity of stars ($g_{\rm WFC} - K_{\rm s} \simeq$ 4.5-5.5) in the original definition. As a result of additional Pleiades (Rees et al. in preparation) and Praesepe observations (see Section 6.1.1) this region is now better sampled. This modification does not affect the resultant semi-empirical model isochrones in the optical INT-WFC colours, and therefore does not change the conclusions of Paper II. Furthermore, it also ensures that any isochrones involving the $K_{\rm s}$ band are now more representative than previous formulations.

We note that although defining a locus by eye is somewhat of a subjective process, the cluster sequence in each photometric system is sufficiently populated and well defined that the uncertainties introduced into the position of the single-star locus are minimal. The overriding source of uncertainty comes from the membership catalogues we have adopted to select cluster members. However, as these are based on a combination of photometric and kinematic diagnostics, coupled with the fact that we have selected members with high probabilities, we are confident that the single-star sequences given in Tables 3 and 4 are accurate to within a few hundredths of a magnitude.

Comparing our Pleiades single-star sequence in the $BVI_{\rm c}K_{\rm s}$ bandpasses to that of Stauffer et al. (2007), in addition to an updated formalism in Kamai et al. 2014, (both of whom also defined the single-star sequence by eye), we notice that our definition is almost identical to both across all bandpasses, expect for small regions where we find differences of the order of <0.05 mag in colour at a given magnitude. We note that such differences are *not* systematic

Table 4. The Praesepe single-star sequence in the SDSS *griz* and 2MASS $K_{\rm s}$ bandpasses. Note that these are apparent magnitudes and hence independent of the assumed distance and reddening. The full table is available as Supporting Information with the online version of the paper; a sample is shown here as a representation of its content.

g	r	i	z	$K_{\rm s}$
15.330	14.009	13.467	13.156	11.143
15.385	14.056	13.501	13.182	11.166
15.440	14.102	13.535	13.208	11.190
15.496	14.148	13.570	13.234	11.213
15.551	14.194	13.604	13.260	11.236
15.606	14.241	13.638	13.286	11.259
15.661	14.287	13.673	13.312	11.282
15.717	14.333	13.707	13.338	11.305
15.772	14.379	13.742	13.364	11.328
15.827	14.426	13.776	13.390	11.351

Table 3. The Pleiades single-star sequence in the combined Johnson–Cousins, 2MASS and INT-WFC bandpasses. Note that these are apparent magnitudes and hence independent of the assumed distance and reddening. The full table is available as Supporting Information with the online version of the paper; a sample is shown here as a representation of its content. Note that the single-star sequence extends further in the $(RI)_{\rm c}$ and $(iZ)_{\rm WFC}$ bandpasses (compared to the bluer optical and near-IR 2MASS bandpasses). Hence there becomes a point along the sequence where we are unable to tie both the $(RI)_{\rm c}$ and $(iZ)_{\rm WFC}$ values to the $K_{\rm s}$-band values. Due to significant colour effects between the two photometric systems, at this point we choose to simply extend the $(iZ)_{\rm WFC}$ sequence, but break the $(RI)_{\rm c}$ sequence and append the remaining values to the end of the table.

B	$g_{\rm WFC}$	V	$r_{\rm WFC}$	$R_{\rm c}$	$i_{\rm WFC}$	$I_{\rm c}$	$Z_{\rm WFC}$	J	H	$K_{\rm s}$
11.384	10.983	10.700	10.514	10.322	10.398	9.957	10.372	9.482	9.177	9.076
11.501	11.091	10.800	10.609	10.414	10.483	10.042	10.450	9.559	9.243	9.138
11.619	11.198	10.900	10.702	10.504	10.567	10.126	10.528	9.633	9.306	9.198
11.737	11.302	11.000	10.793	10.595	10.649	10.210	10.604	9.705	9.368	9.256
11.854	11.407	11.100	10.882	10.684	10.729	10.294	10.678	9.775	9.428	9.313
11.973	11.508	11.200	10.969	10.774	10.807	10.376	10.750	9.841	9.484	9.367
12.092	11.607	11.300	11.053	10.862	10.883	10.458	10.820	9.904	9.538	9.419
12.210	11.708	11.400	11.139	10.951	10.959	10.540	10.890	9.966	9.591	9.470
12.329	11.806	11.500	11.220	11.038	11.032	10.620	10.957	10.024	9.640	9.518
12.448	11.907	11.600	11.304	11.125	11.106	10.699	11.025	10.082	9.689	9.565

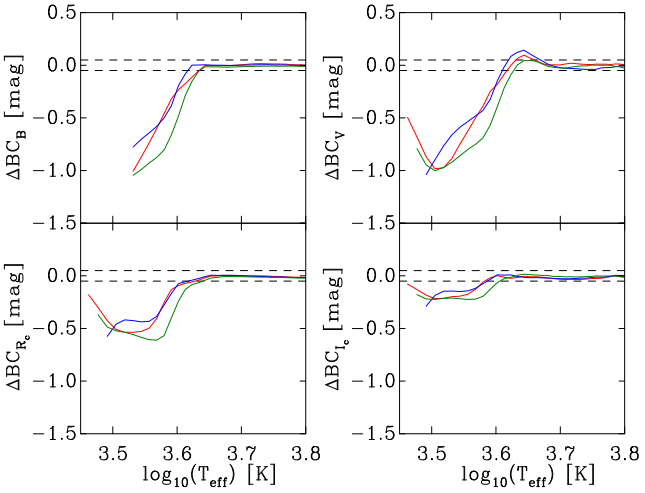

Figure 3. Model-dependent corrections (ΔBC, defined as $BC_{empirical} - BC_{theory}$) calculated as a function of T_{eff} for the optical $BV(RI)_c$ Johnson–Cousins bandpasses. Corrections are shown for the following models: BCAH98 $\alpha = 1.9$ (red), DCJ08 (blue) and updated Pisa (green). The dashed lines represent the ± 0.05 mag level with respect to zero.

over the entire colour range of the Pleiades data set, but are instead localized to regions with a relative paucity of stars. We can therefore estimate what effect such localized differences in the single-star sequence has on our age scale by translating the difference in colour at a given magnitude into a fractional difference in age. For a difference (e.g. in the $V - I_c$ colour) of 0.05 mag, we find that this equates to a difference in age of $\lesssim$10 per cent. Hence, this represents the systematic uncertainty in our age scale (within specific narrow colour ranges) as a result of adopting our own definition of the Pleiades single-star sequence instead of others available in the literature.

In Papers I and II, we described the process of deriving empirical BCs at each point along the fiducial locus and then expressing this as a correction (ΔBC) to the theoretical BC derived for the appropriate T_{eff} and $\log g$ for that point in the sequence. In Paper I, we used binary systems with well-constrained dynamical masses to demonstrate that the models fit the K_s-band flux well. We can then use this to set the T_{eff} at each point along our fiducial locus (this also ensures that we have a well-defined mass scale tied to that of the adopted sequence). Looking, for instance, at the K_s, $V - K_s$ CMD, the necessary ΔBC_V can be determined by calculating the difference between the fiducial locus and the model isochrone at a given T_{eff}. Repeating this process over the colour range of the fiducial locus or T_{eff} range of the model isochrone (whichever is more restrictive) results in a set of T_{eff}-dependent ΔBC_Vs. These corrections can then be added to the theoretical BC grid (which is a function of T_{eff} and $\log g$) at the appropriate T_{eff} irrespective of its $\log g$, thereby defining a set of $\log g$-dependent semi-empirical BC_Vs. This process can be extended to calculate model-dependent ΔBCs in other bandpasses. As demonstrated in Paper I, the models match the observed shape of the Pleiades locus at $T_{eff} \gtrsim 4300$ K, and hence we only apply ΔBCs to the theoretical BC–T_{eff} relation below this T_{eff}. As an illustration, in Fig. 3, we show the derived model-dependent ΔBCs in the Johnson–Cousins photometric system. A full discussion on the quantification of the observed discrepancy and the effect this has on the derived ages for young stars in this T_{eff} regime is given in Paper I.

This process was repeated for each of the three sets of evolutionary models in the four photometric systems (we create the corresponding IPHAS/UVEX semi-empirical BC–T_{eff} relations by applying the transformations given in Table 1 to the derived relations in the INT-WFC system). Both the BCAH98 $\alpha = 1.9$ and the updated Pisa models are only available in solar metallicities; however, Praesepe has a slightly supersolar composition (see Section 4.2). Thus, for these models, we simply overlay supersolar atmospheres ($1.2\,Z_\odot$) on the solar composition interior models and calculate the corrections to the BCs as described above. We shall consider the effects of this in Section 6.2. The DCJ08 models, however, are available in supersolar metallicities, so for these we perform a quadratic interpolation (as in Section 4.2) to create a grid of $1.2\,Z_\odot$ interior models and then combine these with the $1.2\,Z_\odot$ atmospheric models. Note that as we have used the K_s-band magnitude of the pre-MS model isochrones as a proxy for T_{eff}, each set of pre-MS interior models requires a slightly different set of semi-empirical BCs to fit the fiducial locus in CMD space. This is due to variations in the underlying physical inputs and assumptions in the models, however, we find that the resultant semi-empirical BC–T_{eff} relations agree to within 0.15 mag at a given T_{eff} across all colours (see e.g. Fig. 4).

Due to exposure time limits for individual fields-of-view in the SDSS, the Praesepe locus only enables us to recalibrate the colour–T_{eff} relation to a limit of $g - i \simeq 3.5$. In comparison, our Pleiades locus in the INT-WFC photometric system extends to $(g - i)_{WFC} \simeq 4.0$. The ΔBCs for each system are significantly different at $\simeq$3900 K (e.g. $\Delta BC_g - \Delta BC_{g_{WFC}} \sim 0.1$ mag), however, they converge towards 3400 K (e.g. $\Delta BC_g - \Delta BC_{g_{WFC}} = 0.04$ mag). Thus, to extend our semi-empirical model isochrones to lower T_{eff} in the SDSS system, we adopt the ΔBCs we have derived for the INT-WFC system and apply these to the equivalent SDSS *griz* bandpasses. Although this is not an ideal solution, it does allow us to extend the semi-empirical SDSS model isochrones to $T_{eff} \simeq 3100$ K, which is a significant advantage and certainly constitutes a marked improvement over adopting purely theoretical model isochrones at such T_{eff}.

5.2 Comparison with empirical colour–T_{eff} relations

Having derived a set of $\log g$-dependent semi-empirical BC–T_{eff} relations in Section 5.1, we can now compare these to empirical colour–T_{eff} relations available in the literature. The Johnson–Cousins system is, at least historically, the most commonly used photometric system and as such there are several independent relations with which to compare against. Given that the majority of the empirical relations in the literature are based on observations of MS stars, we therefore adopt semi-empirical isochrones with ages of 1 Gyr for this comparison. Even though we derived the ΔBCs in the Johnson–Cousins system using the observed colours of Pleiades members, and hence pre-MS objects at the lowest masses, we have applied the derived ΔBC at a specific T_{eff} to all values of $\log g$ at that T_{eff} (see Assumption 2 in Section 1.2). Thus, we can create semi-empirical isochrones across a wide range of ages, and subsequently $\log g$, and not just a narrow range close to that of the fiducial cluster.

Fig. 4 shows how the semi-empirical BC–T_{eff} relations, as defined by semi-empirical model isochrones with ages of 1 Gyr, compare with several well-known empirical relations, namely those of Kenyon & Hartmann (1995),[4] VandenBerg & Clem (2003),

[4] These relations in fact constitute a compilation of adopted relations from the then current literature and were taken from Johnson (1966), Schmidt-Kaler (1982), Bessell & Brett (1988) and Bessel (1990).

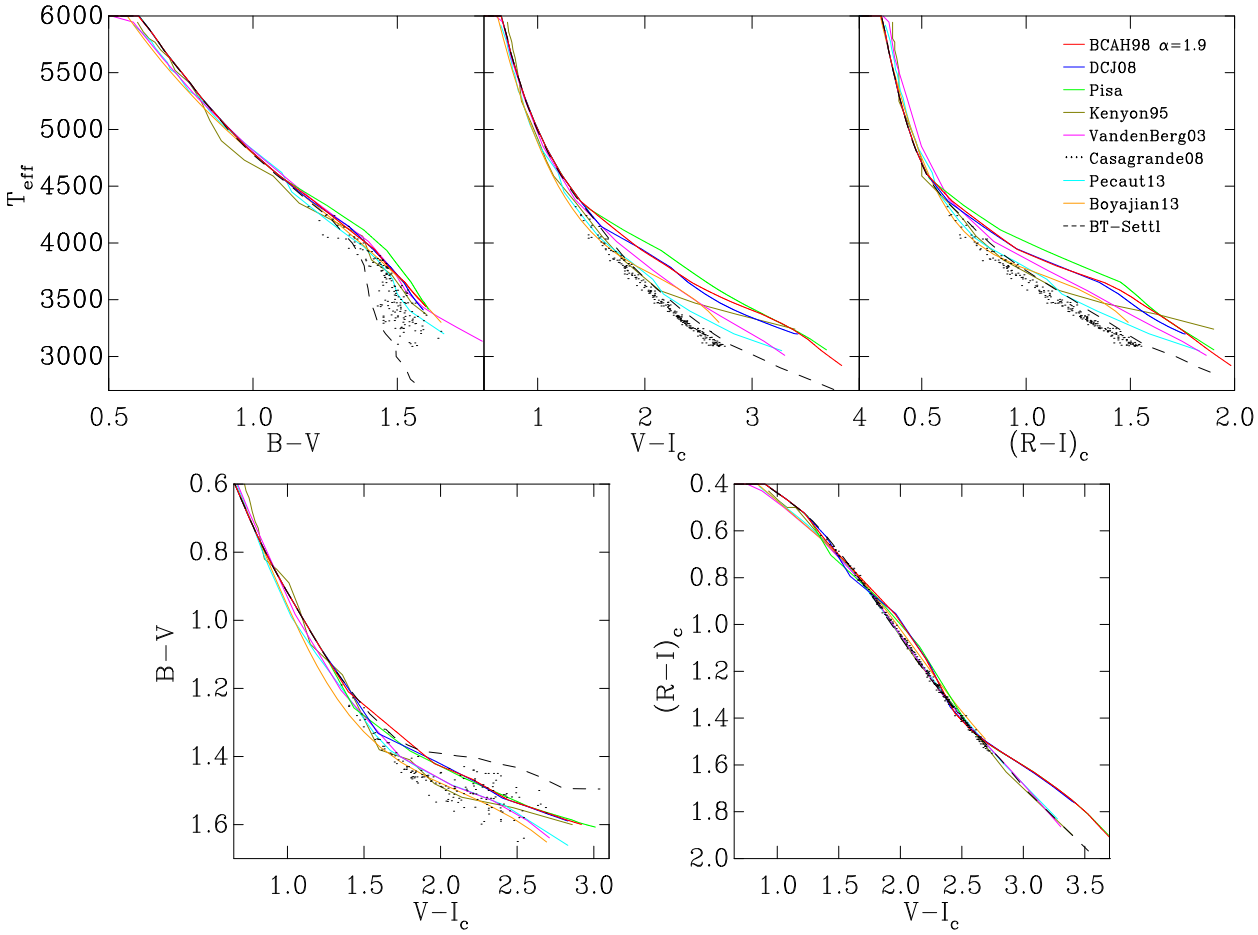

Figure 4. Colour–$T_{\rm eff}$ and colour–colour relations in the Johnson–Cousins photometric system created using semi-empirical pre-MS model isochrones at an age of 1 Gyr. In each panel, the relations derived using the BCAH98 $\alpha = 1.9$ (red), DCJ08 (blue) and updated Pisa models (green) are shown in addition to the empirical relations of Kenyon & Hartmann (1995) (dwarf stars; olive), VandenBerg & Clem (2003) (dwarf stars; magenta), Casagrande et al. (2008) (dwarf stars with mixed metallicity; black dots), Pecaut & Mamajek (2013) (dwarf stars; cyan) and Boyajian et al. (2013) (dwarf stars; orange). Note that the Casagrande et al. (2008) sample represents another empirical formalism, however, due to metallicity effects (especially in the $B - V$ colour) a polynomial was not fitted through the sequence, and thus we retain them as individual points. For reference, we also plot the theoretical relation derived using the BT-Settl models at a $\log g = 4.5$ (black dashed).

Casagrande, Flynn & Bessell (2008), Pecaut & Mamajek (2013) and Boyajian et al. (2013). As a reference, in Fig. 4 we also plot the theoretical colour–$T_{\rm eff}$ and colour–colour relations predicted by the PHOENIX BT-Settl models for $\log g = 4.5$. We note that the Casagrande et al. (2008) sample represents another empirical formalism, and should not be considered as data against which the various colour–$T_{\rm eff}$ and colour–colour relations shown in Fig. 4 should be compared against. Due to metallicity effects (especially in the $B - V$ colour, see below) a polynomial was not fitted through the sequence, and thus we retain them as individual points in Fig. 4.

From the upper panels of Fig. 4 it is clear that, even amongst the empirical relations, in the low-temperature regime there is considerable scatter in the colour one would adopt for a given $T_{\rm eff}$ (as large as 1 mag in $V - I_{\rm c}$ at $T_{\rm eff} \simeq 3200$ K). What is noticeable, however, is that the relations of VandenBerg & Clem (2003) and Pecaut & Mamajek (2013) appear to most closely match the observed shape of the Casagrande et al. (2008) sample, whereas the Boyajian et al. (2013) relation appears to lie somewhere in-between these two formalisms and the Kenyon & Hartmann (1995) relation diverges [especially in the $V - I_{\rm c}$ and $(R - I)_{\rm c}$ planes] from the other empirical relations at $T_{\rm eff} \lesssim 3500$ K. Furthermore, it is evident that the spread in the Casagrande et al. (2008) sample is significantly larger in the $B - V$ plane compared to the $V - I_{\rm c}$ and $(R - I)_{\rm c}$ planes which is suggestive of a strong metallicity effect in the $B - V$ colour index that is not present at longer wavelengths (see also Ramírez & Meléndez 2005; Casagrande et al. 2010). Also evident from Fig. 4 is that the theoretical $B - V$ colour–$T_{\rm eff}$ relation from the BT-Settl models is too blue compared to the other empirical relations.

The colour–colour relations plotted in the lower panels of Fig. 4 imply that whilst the colour scales of these empirical relations are likely reliable, constraining the $T_{\rm eff}$ scale, especially at low temperatures, is much more problematic. This fact is reflected in the various methods which have been adopted to derive the $T_{\rm eff}$ scales for cool stars in these relations, including visually fitting blackbody curves to observed data (Kenyon & Hartmann 1995, see also Johnson 1966), a modified infrared flux method (Casagrande et al. 2008), multiband spectral energy distribution fitting (Pecaut & Mamajek 2013) and direct measurement of angular diameters (Boyajian et al. 2013). It is interesting to note that despite the significant differences between the various empirical $V - I_{\rm c}$ and $(R - I)_{\rm c}$ colour–$T_{\rm eff}$ relations, the $V - I_{\rm c}$, $(R - I)_{\rm c}$ colour–colour relation shows remarkable agreement between the various formalisms.

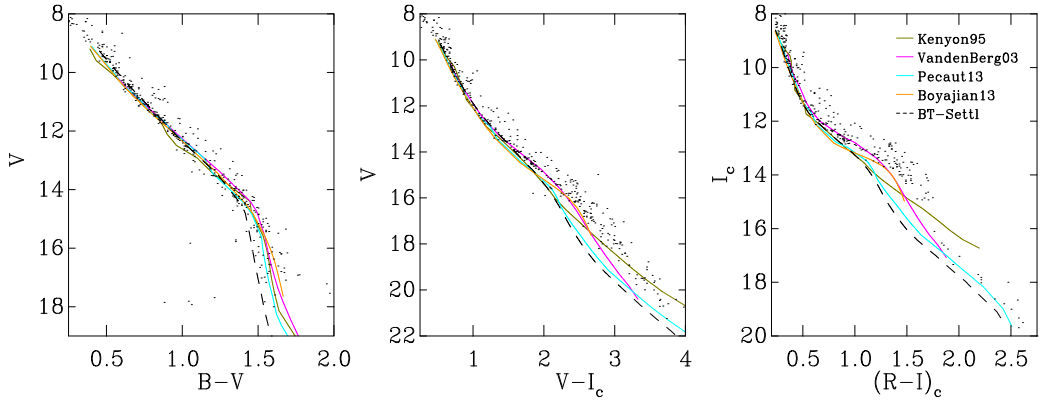

Figure 5. Optical CMDs of Pleiades members in the Johnson–Cousins photometric system. Left: V, $B-V$ CMD. Middle: V, $V-I_c$ CMD. Right: I_c, $(R-I)_c$ CMD. Overlaid are 130 Myr BCAH98 $\alpha = 1.9$ pre-MS model isochrones transformed into CMD space using the empirical BCs and colour–$T_{\rm eff}$ relations of Kenyon & Hartmann (1995, olive), VandenBerg & Clem (2003, magenta), Pecaut & Mamajek (2013, cyan) and Boyajian et al. (2013, orange). Note that Boyajian et al. (2013) do not provide empirical BCs with their colour–$T_{\rm eff}$ relations and therefore we adopt the dwarf BC$_V$–$T_{\rm eff}$ relation of Pecaut & Mamajek (2013). In each panel, we have adopted a distance modulus $dm = 5.63$ mag and a reddening of $E(B-V) = 0.04$ mag [equivalent to $E(V-I_c) = 0.05$ mag and $E(R_c - I_c) = 0.03$ mag]. For reference, we also plot a 130 Myr BCAH98 $\alpha = 1.9$ model isochrone transformed using the BT-Settl atmospheric models (black dashed).

Although our colour–$T_{\rm eff}$ relations are much redder than the other relations shown in Fig. 4, the relations we have derived are those required to transform a given pre-MS interior model so as to follow the observed fiducial locus in various CMDs, i.e. they represent the necessary corrections to make the models work better. As we have combined both the interior and atmospheric models to calculate theoretical colours and magnitudes, the derived discrepancy between the models and the data cannot simply be attributed to one or the other. Instead, it is a combination of the uncertainties at low $T_{\rm eff}$ associated with both sets of models, and likely includes contributions from the atmospheric models (e.g. incomplete opacity sources) and interior models (e.g. treatment of convection) in addition to physical processes which affect the data, but are not included in the models (e.g. magnetic activity).

In Fig. 5, we further demonstrate the observed scatter between the different empirical colour–$T_{\rm eff}$ relations by using these to transform a 130 Myr BCAH98 $\alpha = 1.9$ model isochrone into various optical CMDs and compare these against our Pleiades catalogue (described in Section 2.1). For this comparison, we adopted the distance and reddening values stated in Section 4.1. Note that Boyajian et al. (2013) do not provide empirical BCs with their colour–$T_{\rm eff}$ relations and therefore we adopt the dwarf BC$_V$–$T_{\rm eff}$ relation of Pecaut & Mamajek (2013).

It is clear that of the empirical relations tested, those of VandenBerg & Clem (2003) provide the closest match to the observed shape of the Pleiades locus, followed by those of Boyajian et al. (2013), whilst those of Kenyon & Hartmann (1995) and Pecaut & Mamajek (2013) show significant deviations. It is interesting to note that all the relations appear to model the Pleiades locus similarly well in the V, $B-V$ CMD, whereas in all the CMDs the theoretical BT-Settl relations predict colours that are too blue (see also Baraffe et al. 1998, who demonstrated this effect for previous generations of PHOENIX atmospheric models).

6 FACTORS AFFECTING THE USE OF PRAESEPE IN PLACE OF THE PLEIADES

In Section 2.4, we highlighted two possible factors which need to be considered when adopting Praesepe (as opposed to the Pleiades) as a fiducial cluster. First, there is the question of enhanced magnetic activity at younger ages, i.e. when we compare the loci of the Pleiades and Praesepe in different CMDs do we see the same effects as noted by Stauffer et al. (2003, see also Kamai et al. 2014)? Secondly, what systematic residuals are introduced by using a stellar locus with a supersolar metallicity to recalibrate solar composition pre-MS model isochrones?

6.1 Effects of enhanced magnetic activity

Enhanced levels of magnetic activity, especially amongst younger stars, can inhibit the convective flows to the stellar surface and result in star spots covering a large fraction of the photosphere (Strassmeier 2009). Depending on the areal coverage of such spots, the observed colours can be somewhat different from older stars of the same $T_{\rm eff}$. An additional consequence of the inhibited convective flows is that the radii of stars with intense magnetic fields can be significantly inflated in comparison to stars of a similar mass but with a much weaker field (e.g. Chabrier, Gallardo & Baraffe 2007; Yee & Jensen 2010). It is beyond the scope of this paper to discuss these processes in too fine a detail, as we are primarily concerned with whether they could introduce systematic differences into the positions of the Praesepe locus (when compared to that of the Pleiades) in the CMD, and therefore introduce possible biases into the calculated ΔBCs.

Stauffer et al. (2003) identified a colour anomaly for K dwarfs in the Pleiades (see also Jones 1972; Mermilliod et al. 1992; Kamai et al. 2014) which is present in both the V, $B-V$ and V, $V-K$ CMDs, but vanishes in the V, $V-I$ CMD. They attributed these differences to a combination of rapid rotation and the presence of star spots on the stellar surface, both of which are observed to become less pronounced with age. Thus, given that we have adopted Praesepe as our fiducial cluster in the SDSS photometric system, we must therefore ask whether we still observe the effects noted by Stauffer et al. (2003) in the equivalent g, $g-i$ and g, $g-K_s$ CMDs.

6.1.1 *CMD comparison of the Pleiades and Praesepe*

As discussed in Section 2.4, Pleiades data are not available in the SDSS photometric system. Therefore, if we are to compare the

Table 5. The central coordinates for each field of view and exposure times in the INT-WFC bandpasses for the observations of Praesepe.

Field	RA Dec. (J2000.0)	Bandpass	Exposure time (s) ×1 unless stated
Praesepe Field A	$08^{h}40^{m}46\overset{s}{.}7$ $+19°32'56\overset{''}{.}0$	g_{WFC}	1, 10(×3), 100
		r_{WFC}	1, 10(×3)
		i_{WFC}	1, 10(×3), 100
Praesepe Field B	$08^{h}40^{m}22\overset{s}{.}7$ $+19°59'59\overset{''}{.}6$	g_{WFC}	1, 10(×3)
		r_{WFC}	1, 10(×3)
		i_{WFC}	1, 10(×3)

sequences of the Pleiades and Praesepe in CMD space to see whether the effect noted by Stauffer et al. (2003) is present in either the g, $g-i$ or g, $g-K_s$ CMD, we must do so in the natural photometric system of the INT-WFC. Whilst there are differences between the SDSS and INT-WFC response functions (see Paper I), they are similar enough that the conclusions based on a comparison in the INT-WFC colours will likely be valid for the SDSS colours.

Observations of two fields within Praesepe (see Table 5) were taken with the 2.5-m INT on La Palma on the nights of 2012 December 5 and 2013 November 11. We used the same instrumentation and filter set on both occasions, and we refer the reader to Paper I for details on these as well as our observational techniques, photometric calibration, data reduction and astrometric calibration. Only the 2013 data were taken in photometric conditions and thus standard star fields in Stripe 82 of the SDSS were observed throughout the night. To create our final optical catalogue, the 2012 and 2013 data were reduced separately and a normalization process (see Naylor et al. 2002, Paper I) performed on the two separate catalogues. The zero-point shift required for each field (effectively allowing for small variations between fields observed on different nights) is a reliable indicator of the internal consistency of the photometry, as well as the accuracy with which the profile corrections was performed, and suggests an accuracy of better than 2 per cent in all bandpasses. Our full Praesepe photometric catalogue is given in Table 6.

We adopt the same Kraus & Hillenbrand (2007) members as described in Section 2.4 to isolate Praesepe members and we present these in the natural INT-WFC photometric system in Table 7. For the Pleiades and Praesepe, we use the distance and reddening values stated in Sections 4.1 and 4.2, respectively. We derive the extinction in each bandpass for both clusters using the extinction grids which we discuss in detail in Section 7.1 and which are created using the atmospheric models, the INT-WFC system responses and the Galactic reddening law of Fitzpatrick (1999). Note that over the colour range of the available photometric data, in addition to the low reddening affecting both clusters, the derived extinction values are insensitive to the adopted T_{eff} and $\log g$, and are affected at only the few mmag level.

Fig. 6 compares the loci of the Pleiades and Praesepe in the $M_{g_{WFC}}, (g-i)_{WFC,\circ}$, $M_{i_{WFC}}, (r-i)_{WFC,\circ}$ and $M_{g_{WFC}}, (g_{WFC}-K_s)_\circ$ CMDs. The Pleiades members are those we identified in Paper I. As noted in Stauffer et al. (2003, see also Kamai et al. 2014), the low-mass Pleiades locus in the $V, B-V$ CMD appeared systematically bluer than that of Praesepe and redder in the $V, V-K_s$ CMD. From Fig. 6, we find no evidence of a significant difference between the two loci in any of the CMDs. This is rather surprising, especially in the $M_{g_{WFC}}, (g-i)_{WFC,\circ}$ CMD, given that the g_{WFC} band has a significant wavelength overlap with the Johnson B band. We note, however, that in the $M_{i_{WFC}}, (r-i)_{WFC,\circ}$ and $M_{g_{WFC}}, (g_{WFC}-K_s)_\circ$ CMDs there may be tentative evidence of small <0.1 mag differences in colour at a given magnitude. These differences are typically smaller than those discussed in the studies of Stauffer et al. (2003) and Kamai et al. (2014), and are associated with regions in the loci of low stellar density. Additional photometric observations of both clusters would be required before we can ascertain whether these differences are indeed genuine variations between the two loci or simply selection effects due to our current photometric coverage of each cluster.

As highlighted in Stauffer et al. (2003), the anomalous $B-V$ colours may be due to an enhanced blue continuum, especially at wavelengths less than $\simeq$4200 Å. Hence, the reason we may not be observing this effect could be due to the fact that, compared to the g_{WFC} band, the Johnson B band is bluer (blue wavelength cut-off $\simeq$3600 Å, cf. $\simeq$4000 Å), more skewed to the blue (maximum throughput at $\simeq$4000 Å, cf. $\simeq$5000 Å) and somewhat narrower ($\simeq$900 Å at 50 per cent throughput, cf. $\simeq$1200 Å). Thus, the presence of plages which could affect B-band photometry may not be observed in g_{WFC}-band observations. Furthermore, although the two

Table 6. A sample of the full Praesepe photometric catalogue with colours and magnitudes in the natural INT-WFC photometric system. Due to space restrictions, we only show the g_{WFC} and $(g-i)_{WFC}$ colours and magnitudes as a representation of its content. The full photometric catalogue (available as Supporting Information with the online version of the paper) also includes photometry in the $(r-i)_{WFC}$ colour and the r_{WFC} and i_{WFC} magnitudes. Columns list unique identifiers for each star in the catalogue: field and CCD number (integer and decimal), ID, RA and Dec. (J2000.0), CCD pixel coordinates of the star, and for each of g_{WFC} and $(g-i)_{WFC}$ there is a magnitude, uncertainty on the magnitude and a flag (OO represents a 'clean detection'; see Burningham et al. 2003 for a full description of the flags.)

Field	ID	RA (J2000.0)	Dec. (J2000.0)	x	y	g_{WFC}	$\sigma_{g_{WFC}}$	Flag	$(g-i)_{WFC}$	$\sigma_{(g-i)_{WFC}}$	Flag
1.04	12	08 40 56.294	+19 34 49.25	602.610	1641.420	8.387	0.010	OS	−0.191	0.014	SS
1.02	4	08 39 56.450	+19 33 10.98	2082.593	813.918	8.415	0.010	OS	−0.094	0.014	SS

Table 7. A sample of the catalogue of colours and magnitudes in the natural INT-WFC photometric system for Praesepe members. The columns and content are in the same format as Table 6. The full photometric catalogue is available as Supporting Information with the online version of the paper.

Field	ID	RA (J2000.0)	Dec. (J2000.0)	x	y	g_{WFC}	$\sigma_{g_{WFC}}$	Flag	$(g-i)_{WFC}$	$\sigma_{(g-i)_{WFC}}$	Flag
2.02	12	08 39 03.549	+19 59 59.20	873.852	1047.167	9.174	0.010	OS	0.396	0.014	SS
2.03	22	08 40 52.437	+20 15 59.48	293.658	758.948	9.214	0.010	OS	0.415	0.014	SS

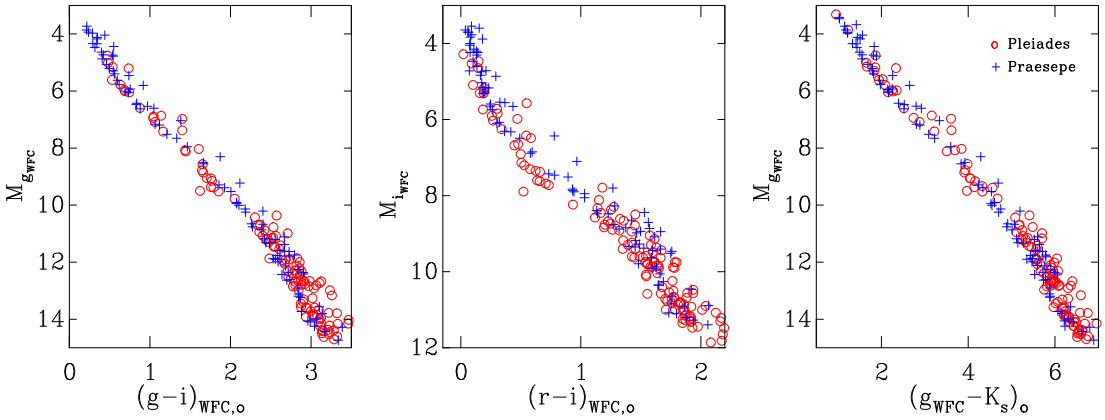

Figure 6. Comparison of the Pleiades (red circles) and Praesepe (blue crosses) members in CMDs. Left: $M_{g_{WFC}}$, $(g-i)_{WFC,\circ}$ CMD. Middle: $M_{i_{WFC}}$, $(r-i)_{WFC,\circ}$ CMD. Right: $M_{g_{WFC}}$, $(g_{WFC}-K_s)_\circ$. There is no indication of systematic differences between the two loci at low masses in any of the CMD.

loci are indistinguishable in the $M_{g_{WFC}}$, $(g-i)_{WFC,\circ}$ (when compared to the V, $B-V$) CMD, this could still be consistent with the presence of star spots as the observed effect depends entirely on the adopted spot-to-star contrast (Jackson & Jeffries 2014). The lack of significant difference between the two loci at lower masses in the $M_{g_{WFC}}$, $(g_{WFC}-K_s)_\circ$ CMD disfavours the idea that pre-MS stars are simply inflated by magnetic activity (the active stars would appear much redder), but is consistent with inflation due to the presence of star spots (see e.g. Jackson & Jeffries 2014).

6.2 Effects of metallicity on semi-empirical BC-$T_{\rm eff}$ relations

The stellar properties predicted by evolutionary models strongly depend on the opacity – and hence metallicity – of the stellar interior as this will dictate how the convective energy transfer propagates through the stellar interior. For example, as the metallicity increases so does the opacity, and therefore for an isochrone of a given age, the position in the Hertzsprung–Russell (HR) diagram will be fainter and cooler when compared to a similarly aged isochrone with a lower metallicity (see e.g. Tognelli et al. 2011). Not only is the luminosity of an isochrone strongly dependent upon metallicity, but in the CMD the degree of sensitivity further depends on the combination of magnitude and colour index adopted. At low temperatures ($T_{\rm eff} \lesssim 3500$ K) molecular species start to become the dominant source of opacity in stellar atmospheres, resulting in noticeable modification to the emergent spectrum. Hence, given the main sources of opacity in this $T_{\rm eff}$ regime (e.g. TiO and VO in the optical, and H_2O in the IR) it is clear that variations in the metallicity could result in appreciable differences to both the stellar spectra and atmospheric structure, and ultimately the observed colours.

The metallicity of Praesepe (in comparison to that of the Pleiades) is approximately 20 per cent supersolar. Unfortunately, the BCAH98 $\alpha = 1.9$ and the updated Pisa models are not available in supersolar compositions. Given that we are limited to solar metallicity interiors, we require an estimate of the effect that using these interiors would have on the semi-empirical BC–$T_{\rm eff}$ relations. There are two possible effects which we must consider. First, given this 20 per cent difference between the metallicities of the Pleiades and Praesepe, how much of a difference does this make to the interior models and what systematic errors could we introduce into the semi-empirical model isochrones? Secondly, is the physical process

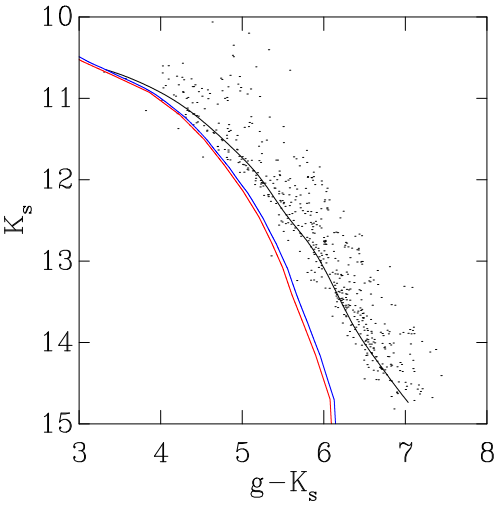

Figure 7. The effects of different metallicity interior models in the K_s, $g-K_s$ CMD of Praesepe members. Overlaid are two 665 Myr theoretical (not semi-empirical) DCJ08 model isochrones adopting a distance modulus $dm = 6.32$ mag and a reddening equivalent to $E(B-V) = 0.027$ mag. Both model isochrones have been transformed into CMD space using supersolar ($1.2\,Z_\odot$) atmospheric models, however, the interior models are solar metallicity ($Z_\odot$; red) and supersolar ($1.2\,Z_\odot$; blue). The black line represents the spline fit to the Praesepe single-star sequence.

which is responsible for the ΔBCs (when comparing the models and the data in CMDs) strongly dependent on metallicity?

6.2.1 *Effects of metallicity on stellar interior models*

Higher metallicity DCJ08 models are available and this therefore allows us to test the effects of metallicity variations on the derived semi-empirical BC–$T_{\rm eff}$ relations. Fig. 7 shows the Praesepe single-star sequence (as given in Table 4) overlaid on the Praesepe members as defined by Kraus & Hillenbrand (2007) in the K_s, $g-K_s$ CMD. We used the positions from Kraus & Hillenbrand (2007) to extract 2MASS photometry for each source from the 2MASS Point Source Catalogue (Cutri et al. 2003). Also plotted in the CMD are two 665 Myr DCJ08 model isochrones; a solar interior model transformed using appropriately supersolar ($1.2\,Z_\odot$) atmospheric models (red) and a supersolar ($1.2\,Z_\odot$) interior transformed using

the same supersolar atmospheric models (blue). Given that we are unable to derive ΔBCs for fiducial sequences of different metallicity in the SDSS system, the DCJ08 model isochrones shown in Fig. 7 are theoretical, i.e. not semi-empirical models.

We can quantify the effect that using solar metallicity interior models would have on the derived BC–$T_{\rm eff}$ relations by calculating the difference in the colour index at a fixed $K_{\rm s}$-band magnitude. In the $T_{\rm eff}$ range where we calculate empirical BCs using observed stellar colours, we calculate that the maximum difference between the colour indices is $[g - K_{\rm s}]_{1.2{\rm Z}_{\odot}} - [g - K_{\rm s}]_{{\rm Z}_{\odot}} \simeq 0.05$ mag. In absolute terms, such a difference may appear unacceptably large, however, recall that we are recalibrating the model isochrones to correct for a discrepancy of ∼0.8 mag in $g - K_{\rm s}$ at the lowest $T_{\rm eff}$ (see Fig. 7).

Investigating whether this difference is wavelength dependent, we quantified the difference in other colour indices and found it to be $\lesssim$0.05 mag. This then implies that despite adopting solar metallicity interior models to create semi-empirical BC–$T_{\rm eff}$ relations, the resultant semi-empirical model isochrones would have a residual uncertainty of $\lesssim$0.05 mag in the magnitude and $\lesssim$0.07 mag in the colour.

We provide only solar composition semi-empirical SDSS pre-MS model isochrones through the internet server. In the case of the DCJ08 models, where supersolar interior models are available, we calculate the ΔBCs as described in Section 5.1 using supersolar ($1.2\,{\rm Z}_{\odot}$) interior and atmospheric models and apply these to the theoretical solar composition BC grid. Thus, for the semi-empirical DCJ08 model isochrones, we expect the uncertainties in the colours and magnitudes to be smaller than the values quoted above. For both the BCAH98 $\alpha = 1.9$ and updated Pisa models, however, we can only calculate the ΔBCs by combining solar interior and supersolar atmospheric models.

6.2.2 *Effects of metallicity on ΔBC*

Given that we have INT-WFC observations of both the Pleiades and Praesepe, a simple test to investigate whether the physical process responsible for the ΔBCs is strongly dependent upon the metallicity is to use the semi-empirical BC–$T_{\rm eff}$ relation we have derived using the Pleiades (solar composition) to transform a solar metallicity interior model at an age of 665 Myr and overlay it on the Praesepe photometric data.

Fig. 8 is an adaptation of Fig. 6 with two 665 Myr DCJ08 model isochrones overlaid. The continuous line is a solar composition semi-empirical model isochrone (transformed using the semi-empirical BC–$T_{\rm eff}$ relation derived using the Pleiades), whereas the dashed line is a theoretical (not semi-empirical) supersolar ($1.2\,{\rm Z}_{\odot}$) metallicity model isochrone. The reason we combine both photometric data sets is simply to increase the number of stars in our sequence. Due to the small areal coverage of our observations in Praesepe there is a paucity of stars in certain regions along the sequence, and so by combining this with our Pleiades data, we can better assess whether the isochrones represent a good match to the observed sequence.

It is clear from Fig. 8 that the solar composition DCJ08 model isochrone is a good fit to the observed shape of the Praesepe sequence in all colours. Thus, we can be reasonably assured that despite composition discrepancies (again at least at the 20 per cent level) between the photometric data and the model isochrones adopted (see Section 6.2.1), this should not have a significant effect on the age derived from using such isochrones in CMDs.

Note that in Fig. 8 there is an obvious mismatch between the data and the models at low $T_{\rm eff}$. At the age of Praesepe and temperatures below ≃3200 K, the DCJ08 interior models become almost vertical in the H–R diagram (see also Fig. 7). This 'turn-over' in the models is not observed at younger ages, e.g. the Pleiades, and therefore our method of creating semi-empirical BC–$T_{\rm eff}$ relations based on the discrepancy between the models and the data will not account for this effect at older ages. Hence we urge the user to exercise caution if using the semi-empirical DCJ08 model isochrones at old ages and at low $T_{\rm eff}$. This effect is not observed in either the BCAH98 $\alpha = 1.9$ or updated Pisa models.

7 PRE-MS ISOCHRONE SERVER

By construction the semi-empirical pre-MS model isochrones presented here will deliver reliable ages between 600 Myr (the age of Praesepe) and 100 Myr (roughly the age of the Pleiades). The question is how well they will work for younger ages, which amounts to testing our assumption that the theoretical relationship for the change in BC with log g, can be applied to the empirical corrections derived from the Pleiades and Praesepe. The next youngest test we

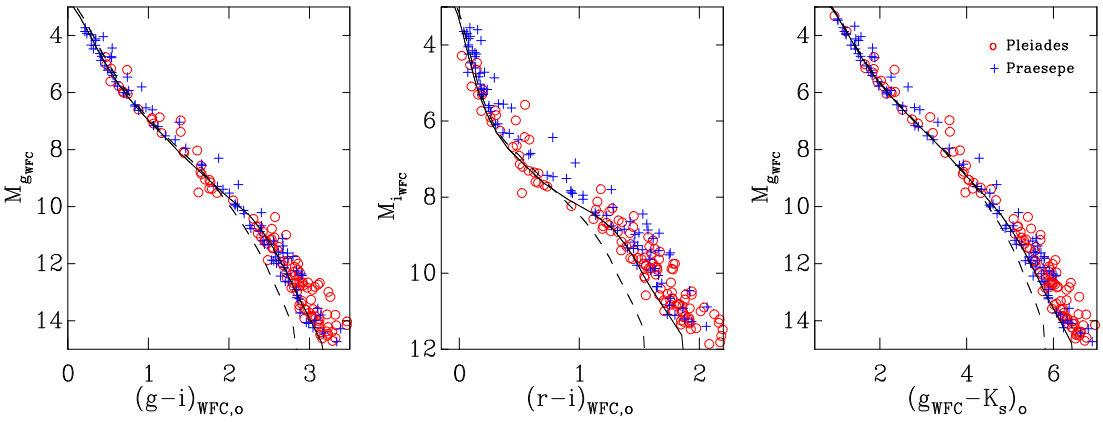

Figure 8. Same as Fig. 6 but demonstrating that ΔBC is not strongly dependent upon metallicity. The continuous line in each panel is a 665 Myr solar composition semi-empirical DCJ08 model isochrone (transformed using the semi-empirical BC–$T_{\rm eff}$ relation derived using the Pleiades). The dashed line is a theoretical (not semi-empirical) supersolar ($1.2\,{\rm Z}_{\odot}$) metallicity DCJ08 model isochrone. The 'turn-over' in both isochrones ($T_{\rm eff} \simeq 3200$ K) is an artefact of the DCJ08 interior models at older ages which is not present at the age of the Pleiades and hence our log g-dependent ΔBCs are unable to account for this.

have is NGC 1960, which has an LDB age of 22 ± 4 Myr (Jeffries et al. 2013), and an upper MS age of $26.3^{+3.2}_{-5.2}$ Myr (Paper II). The isochrones presented here based on the BCAH98 $\alpha = 1.9$ or DCJ08 interior models yield an age of 19–21 Myr (Paper II) in good agreement with the other two age diagnostics. Unfortunately, there are no LDB ages for younger clusters, and thus the only remaining test is the upper MS ages, which typically have large age uncertainties. Of these, however, λ Ori has a rather precise upper MS age of 9–11 Myr (Paper II), which is in good agreement with the ages from the present semi-empirical models isochrones of 10.0–11.0 Myr (BCAH98 $\alpha = 1.9$ interiors) or 7.6–8.7 Myr (DCJ08 interiors). There are five other clusters with ages of between 5 and 15 Myr, where the uncertainties in the upper MS age are of the order of a factor 2, but within these uncertainties the upper MS ages and those for the isochrones in this work agree. Only at around 3 Myr is there significant evidence for a difference between the pre-MS and upper MS ages (Paper II). Thus, the semi-empirical pre-MS model isochrones presented here yield ages in agreement with other methods over the two decades of age from 6 to 600 Myr.

We reiterate the three underlying assumptions that we have adopted in the construction of these semi-empirical model isochrones.

Assumption 1: the theoretical models fit the K_s-band flux well and therefore we can use this to determine the $T_{\rm eff}$ at points along our fiducial locus and derive the necessary corrections.

Assumption 2: the empirical corrections in a given bandpass have the same $\log g$ dependence as the theoretical BCs.

Assumption 3: all clusters are assumed to behave like the Pleiades such that there are no intracluster effects due to, for example, binary fractions and mass ratios, intrinsic age spread, rotation distribution and activity-related effects on the observed colours. It is important that these assumptions are well understood by the reader/user given that our primary aim in making these models available is to allow other users to calculate cluster ages from the pre-MS members which are on a consistent scale with those we have derived (see Paper II). These models are also tailored for identifying possible new members and determining mass functions for stellar populations from their positions in the CMD. Given the methodology of creating these model isochrones, we would advise users *not* to use these models to compare against new photometric observations and then critique either the interior or atmospheric models due to a mismatch between the models and the data.

Our semi-empirical pre-MS model isochrones can be found at http://www.astro.ex.ac.uk/people/timn/isochrones/. The server itself is designed to be self-explanatory and guide the user through the various choices, e.g. pre-MS interior model, mass and age range and photometric system, etc.; however, we would like to provide a little more detail on two points, namely the treatment of the reddening and extinction, and the output of the model isochrones.

7.1 Reddening and extinction

Using the simple formalism we have adopted for deriving the BCs from atmospheric models (see Section 3.2), it is straightforward to then include the effects of both reddening and extinction when creating a model isochrone. As discussed in Paper II (see also Bessell, Castelli & Plez 1998), the reddening and extinction applied to each mass point in a given isochrone is dependent upon the $T_{\rm eff}$ of the star, i.e. for a given amount of intervening material, a larger value of, for example, $E(B-V)$ will be measured from the higher $T_{\rm eff}$ stars than from the lower $T_{\rm eff}$ objects. This therefore leads to differential reddening along the model isochrone and we can account for such effects in the isochrone server by following the method described in Paper II, whereby we construct extinction grids based on the atmospheric models, photometric system bandpasses and a description of the interstellar extinction law.

The atmospheric models were reddened adopting the interstellar extinction law of Fitzpatrick (1999) with $R_V = 3.1$, and folded through the various system responses (see Table 2 for a list). The models were reddened in steps of 0.5 from $E(B-V)_{\rm nom} = 0.0$ to 2.0 mag [where $E(B-V)_{\rm nom}$ represents the amount of interstellar material between an observer and the object], with the grids comprising extinction in the various bandpasses as a function of $T_{\rm eff}$ and $\log g$. Thus to redden an isochrone, the user can specify a specific $E(B-V)$ value and the server will automatically calculate the corresponding $E(B-V)_{\rm nom}$, and subsequently use this to interpolate within the extinction grid for the extinction and reddening for a star of given $T_{\rm eff}$ and $\log g$ in the model isochrone. This process is then repeated along the full mass range of the isochrone.

7.2 Model isochrone output

The standard model isochrone output comprises a single-star sequence consisting of 10 000 points equally sampling a given mass range. The user, however, may also wish to include the effects of binarity, essentially modifying the output from a linear curve in CMD space to a two-dimensional distribution which can then be used to perform statistically robust fitting to photometric data sets (e.g. Cargile & James 2010; Da Rio, Gouliermis & Gennaro 2010b).

We follow the formalism as mentioned in Section 4 (see Paper II for a more complete discussion), whereby we create a two-dimensional distribution using a Monte Carlo method to simulate 10^6 stars over a specific mass range for a given mass function and binary fraction. The mass function we adopt is the canonical broken power-law IMF of Dabringhausen et al. (2008) discussed in Section 4.2. The user can then choose a given binary fraction (between 0.0 and 1.0), and if a generated star happens to be a binary, the companion mass is assigned as described in Section 4. Note that due to lower $T_{\rm eff}$ limits as a result of deriving the empirical BCs (or alternatively mass limits in the interior models) some assigned secondary stars may lie below this lower limit. In such cases, these secondary stars are assumed to make a negligible contribution to the system light, which is equivalent to placing the binary on the single-star sequence. This limitation can lead to a wedge of zero probability between the single- and binary-star sequences at low masses.

8 CONCLUSIONS

We present an isochrone server to make sets of semi-empirical pre-MS isochrones in the Johnson–Cousins, INT-WFC, 2MASS, SDSS and IPHAS/UVEX photometric systems publicly available. The stages we have gone through to achieve this are as follows.

(i) We created fiducial loci in CMD space using photometric data of young clusters with known age, distance and reddening. For the Johnson–Cousins, INT-WFC, 2MASS and IPHAS/UVEX systems we adopted the Pleiades, whereas for the SDSS system we used Praesepe.

(ii) Using the K_s-band magnitude to define the $T_{\rm eff}$ scale along the fiducial loci, we quantified the discrepancy between the observed sequence and theoretical pre-MS model isochrones as a function of $T_{\rm eff}$ in individual photometric bandpasses.

(iii) Semi-empirical pre-MS model isochrones can then be created using existing stellar interior models in conjunction with the

recalibrated BC–$T_{\rm eff}$ relations (assuming a model dependence for $\log g$).

(iv) These new semi-empirical models are made available via the Cluster Collaboration website http://www.astro.ex.ac.uk/people/timn/isochrones/ and the user is able to choose the following inputs: interior model, mass range, age (or age range) and photometric system, as well as include the effects of interstellar reddening and binarity. In the future, we expect to make additional interior models and photometric systems available through this server.

(v) We have investigated the effects of both increased magnetic activity and variations in chemical compositions between using the Pleiades and Praesepe to define our fiducial loci. We find no evidence, through comparison in CMD space, to suggest that one locus is systematically offset with respect to the other. Furthermore, we note that the colours of the semi-empirical pre-MS model isochrones in the SDSS photometric system have residual uncertainties of $\simeq$0.07 mag as a result of the metallicity discrepancy between the Praesepe photometric data and the stellar interior models.

(vi) We have derived new cluster parameters for both the Pleiades and Praesepe, which are on a consistent scale with the MS parameters given in Paper II. Not allowing for systematic uncertainties, we determine ages of 135^{+20}_{-11} and 665^{+14}_{-7} Myr as well as distances of 132 ± 2 and 184 ± 2 pc for the Pleiades and Praesepe, respectively.

ACKNOWLEDGEMENTS

JMR is funded by a UK Science and Technology Facilities Council (STFC) studentship. EEM acknowledges support from the National Science Foundation (NSF) Award AST-1008908. The authors would like to thank Emanuele Tognelli for the updated set of Pisa models and John Stauffer for sharing his catalogue of Kron photometric measurements of Pleiades members. The authors would also like to thank the referee for comments which have vastly improved the clarity of the manuscript.

This research has made use of data obtained at the Isaac Newton Telescope, which is operated on the island of La Palma by the Isaac Newton Group (ING) in the Spanish Observatorio del Roque de los Muchachos of the Institutio de Astrofisica de Canarias. This research has made use of archival data products from the Two-Micron All-Sky Survey (2MASS), which is a joint project of the University of Massachusetts and the Infrared Processing and Analysis Center, funded by the National Aeronautics and Space Administration (NASA) and the National Science Foundation.

This research has made use of public data from the SDSS. Funding for the SDSS was provided by the Alfred P. Sloan Foundation, the Participating Institutions, the National Science Foundation, the US Department of Energy, the National Aeronautics and Space Administration, the Japanese Monbukagakusho, the Max Planck Society and the Higher Education Funding Council for England. The SDSS was managed by the Astrophysical Research Consortium for the Participating Institutions.

REFERENCES

Ahn C. P. et al., 2012, ApJS, 203, 21
Allard F., Homeier D., Freytag B., 2011, in Johns-Krull C., Browning M. K., West A. A., eds, ASP Conf. Ser. Vol. 448, 16th Cambridge Workshop on Cool Stars, Stellar Systems, and the Sun. Astron. Soc. Pac., San Francisco, p. 91
An D., Terndrup D. M., Pinsonneault M. H., Paulson D. B., Hanson R. B., Stauffer J. R., 2007, ApJ, 655, 233
Asplund M., Grevesse N., Sauval A. J., Scott P., 2009, ARA&A, 47, 481
Baraffe I., Chabrier G., Allard F., Hauschildt P. H., 1998, A&A, 337, 403
Baraffe I., Chabrier G., Allard F., Hauschildt P. H., 2002, A&A, 382, 563
Barrado y Navascués D., Stauffer J. R., Jayawardhana R., 2004, ApJ, 614, 386
Bastian N., Covey K. R., Meyer M. R., 2010, ARA&A, 48, 339
Bell C. P. M., Naylor T., Mayne N. J., Jeffries R. D., Littlefair S. P., 2012, MNRAS, 424, 3178 (Paper I)
Bell C. P. M., Naylor T., Mayne N. J., Jeffries R. D., Littlefair S. P., 2013, MNRAS, 434, 806 (Paper II)
Bessel M. S., 1990, A&AS, 83, 357
Bessell M. S., 1979, PASP, 91, 589
Bessell M. S., Brett J. M., 1988, PASP, 100, 1134
Bessell M., Murphy S., 2012, PASP, 124, 140
Bessell M. S., Weis E. W., 1987, PASP, 99, 642
Bessell M. S., Castelli F., Plez B., 1998, A&A, 333, 231
Bidelman W. P., 1956, PASP, 68, 318
Boesgaard A. M., Roper B. W., Lum M. G., 2013, ApJ, 775, 58
Bonatto C., Bica E., Girardi L., 2004, A&A, 415, 571
Bouvier J., Stauffer J. R., Martin E. L., Barrado y Navascues D., Wallace B., Bejar V. J. S., 1998, A&A, 336, 490
Boyajian T. S. et al., 2013, ApJ, 771, 40
Brott I., Hauschildt P. H., 2005, in Turon C., O'Flaherty K. S., Perryman M. A. C., eds, ESA SP-576, The Three-Dimensional Universe with Gaia. ESA, Noordwijk, p. 565
Brown T. M., Ferguson H. C., Smith E., Kimble R. A., Sweigart A. V., Renzini A., Rich R. M., VandenBerg D. A., 2003, ApJ, 592, L17
Brown T. M., Ferguson H. C., Smith E., Kimble R. A., Sweigart A. V., Renzini A., Rich R. M., VandenBerg D. A., 2004, ApJ, 613, L125
Burningham B., Naylor T., Jeffries R. D., Devey C. R., 2003, MNRAS, 346, 1143
Cargile P. A., James D. J., 2010, AJ, 140, 677
Casagrande L., Flynn C., Bessell M., 2008, MNRAS, 389, 585
Casagrande L., Ramírez I., Meléndez J., Bessell M., Asplund M., 2010, A&A, 512, A54
Castelli F., 1991, A&A, 251, 106
Castelli F., Kurucz R. L., 2004, in Piskunov N. E., Weiss W. W., Gray D. F., eds, Proc. IAU Symp. 210, Modelling of Stellar Atmospheres. Astron. Soc. Pac., San Francisco, p. A20
Chabrier G., Gallardo J., Baraffe I., 2007, A&A, 472, L17
Cohen M., Wheaton W. A., Megeath S. T., 2003, AJ, 126, 1090
Cutri R. M., Skrutskie M. F., van Dyk S. et al., 2003, 2MASS Point Source Catalogue, available at: http://www.ipac.caltech.edu/2mass/
Cutri R. M. et al., 2012, VizieR Online Data Catalog: 2MASS 6X Point Source Working Database, II/281
Dabringhausen J., Hilker M., Kroupa P., 2008, MNRAS, 386, 864
Da Rio N., Robberto M., Soderblom D. R., Panagia N., Hillenbrand L. A., Palla F., Stassun K. G., 2010a, ApJ, 722, 1092
Da Rio N., Gouliermis D. A., Gennaro M., 2010b, ApJ, 723, 166
Delfosse X., Forveille T., Ségransan D., Beuzit J., Udry S., Perrier C., Mayor M., 2000, A&A, 364, 217
Dias W. S., Alessi B. S., Moitinho A., Lépine J. R. D., 2002, A&A, 389, 871
Doi M. et al., 2010, AJ, 139, 1628
Dotter A., Chaboyer B., Jevremović D., Kostov V., Baron E., Ferguson J. W., 2008, ApJS, 178, 89
Drew J. E. et al., 2005, MNRAS, 362, 753
Ferguson J. W., Alexander D. R., Allard F., Barman T., Bodnarik J. G., Hauschildt P. H., Heffner-Wong A., Tamanai A., 2005, ApJ, 623, 585
Fitzpatrick E. L., 1999, PASP, 111, 63
Fossati L., Bagnulo S., Landstreet J., Wade G., Kochukhov O., Monier R., Weiss W., Gebran M., 2008, A&A, 483, 891
Gáspár A., Rieke G. H., Su K. Y. L., Balog Z., Trilling D., Muzzerole J., Apai D., Kelly B. C., 2009, ApJ, 697, 1578
González-Solares E. A. et al., 2008, MNRAS, 388, 89
Groot P. J. et al., 2009, MNRAS, 399, 323
Hartmann L., 2003, ApJ, 585, 398
Hauck B., Mermilliod M., 1998, A&AS, 129, 431

Hillenbrand L. A., White R. J., 2004, ApJ, 604, 741
Iglesias C. A., Rogers F. J., 1996, ApJ, 464, 943
Jackson R. J., Jeffries R. D., 2014, MNRAS, 441, 2111
Jeffries R. D., Thurston M. R., Hambly N. C., 2001, A&A, 375, 863
Jeffries R. D., Oliveira J. M., Naylor T., Mayne N. J., Littlefair S. P., 2007, MNRAS, 376, 580
Jeffries R. D., Jackson R. J., James D. J., Cargile P. A., 2009, MNRAS, 400, 317
Jeffries R. D., Naylor T., Mayne N. J., Bell C. P. M., Littlefair S. P., 2013, MNRAS, 434, 2438
Johnson H. L., 1952, ApJ, 116, 640
Johnson H. L., 1966, ARA&A, 4, 193
Johnson H. L., Morgan W. W., 1953, ApJ, 117, 313
Jones B. F., 1972, ApJ, 171, L57
Kamai B. L., Vrba F. J., Stauffer J. R., Stassun K. G., 2014, AJ, 148, 30
Kenyon S. J., Hartmann L., 1995, ApJS, 101, 117
Kraus A. L., Hillenbrand L. A., 2007, AJ, 134, 2340
Lejeune T., Schaerer D., 2001, A&A, 366, 538
Lodieu N., Deacon N. R., Hambly N. C., 2012, MNRAS, 422, 1495
Lyra W., Moitinho A., van der Bliek N. S., Alves J., 2006, A&A, 453, 101
Mamajek E. E., 2012, ApJ, 754, L20
Mayne N. J., Naylor T., 2008, MNRAS, 386, 261
Mayne N. J., Naylor T., Littlefair S. P., Saunders E. S., Jeffries R. D., 2007, MNRAS, 375, 1220
Mendoza E. E., 1967, Bol. Obs. Tonantzintla Tacubaya, 4, 149
Mermilliod J. C., 2006, VizieR Online Data Catalog: Homogeneous Means in the UBV System (Mermilliod 1991), II/168
Mermilliod J.-C., Rosvick J. M., Duquennoy A., Mayor M., 1992, A&A, 265, 513
Moraux E., Bouvier J., Stauffer J. R., 2001, A&A, 367, 211
Naylor T., 2009, MNRAS, 399, 432
Naylor T., Jeffries R. D., 2006, MNRAS, 373, 1251
Naylor T., Totten E. J., Jeffries R. D., Pozzo M., Devey C. R., Thompson S. A., 2002, MNRAS, 335, 291
Oke J. B., Gunn J. E., 1983, ApJ, 266, 713
Pecaut M. J., Mamajek E. E., 2013, ApJS, 208, 9
Pecaut M. J., Mamajek E. E., Bubar E. J., 2012, ApJ, 746, 154
Pinsonneault M. H., Terndrup D. M., Hanson R. B., Stauffer J. R., 2004, ApJ, 600, 946
Ramírez I., Meléndez J., 2005, ApJ, 626, 465
Rogers F. J., Nayfonov A., 2002, ApJ, 576, 1064
Salaris M., Weiss A., Percival S. M., 2004, A&A, 414, 163
Saumon D., Chabrier G., van Horn H. M., 1995, ApJS, 99, 713
Schaller G., Schaerer D., Meynet G., Maeder A., 1992, A&AS, 96, 269
Schmidt-Kaler T., 1982, in Landolt-Börnstein, Neue Serie VI/2b. Springer, Berlin, p. 453, 15
Siess L., Dufour E., Forestini M., 2000, A&A, 358, 593
Skrutskie M. F. et al., 2006, AJ, 131, 1163
Soderblom D. R., Nelan E., Benedict G. F., McArthur B., Ramirez I., Spiesman W., Jones B. F., 2005, AJ, 129, 1616
Soderblom D. R., Laskar T., Valenti J. A., Stauffer J. R., Rebull L. M., 2009, AJ, 138, 1292
Soderblom D. R., Hillenbrand L. A., Jeffries R. D., Mamajek E. E., Naylor T., 2013, in Beuther H., Klessen R., Dullemond C., Henning Th ., eds, Protostars and Planets VI, Ages of Young Stars. Univ. Arizona Press, Tucson, available at: http://www.mpia-hd.mpg.de/homes/ppvi/proc.php
Stauffer J. R., 1980, AJ, 85, 1341
Stauffer J. R., 1982, AJ, 87, 1507
Stauffer J. R., 1984, ApJ, 280, 189
Stauffer J. R., Hartmann L. W., 1987, ApJ, 318, 337
Stauffer J. R., Schild R., Barrado y Navascues D., Backman D. E., Angelova A. M., Kirkpatrick J. D., Hambly N., Vanzi L., 1998, ApJ, 504, 805
Stauffer J. R., Jones B. F., Backman D., Hartmann L. W., Barrado y Navascués D., Pinsonneault M. H., Terndrup D. M., Muench A. A., 2003, AJ, 126, 833
Stauffer J. R. et al., 2007, ApJS, 172, 663
Strassmeier K. G., 2009, A&AR, 17, 251
Taylor B. J., 2006, AJ, 132, 2453
Taylor B. J., Joner M. D., Jeffery E. J., 2008, ApJS, 176, 262
Tognelli E., Prada Moroni P. G., Degl'Innocenti S., 2011, A&A, 533, A109
Tognelli E., Degl'Innocenti S., Prada Moroni P. G., 2012, A&A, 548, A41
van Leeuwen F., 2009, A&A, 497, 209
VandenBerg D. A., Clem J. L., 2003, AJ, 126, 778
Yee J. C., Jensen E. L. N., 2010, ApJ, 711, 303
York D. G. et al., 2000, AJ, 120, 1579

SUPPORTING INFORMATION

Additional Supporting Information may be found in the online version of this article:

Table 3. The Pleiades single-star sequence in the combined Johnson–Cousins, 2MASS and INT-WFC bandpasses.
Table 4. The Praesepe single-star sequence in the SDSS *griz* and 2MASS K_s bandpasses.
Table 6. A sample of the full Praesepe photometric catalogue with colours and magnitudes in the natural INT-WFC photometric system.
Table 7. A sample of the catalogue of colours and magnitudes in the natural INT-WFC photometric system for Praesepe members. (http://mnras.oxfordjournals.org/lookup/suppl/doi:10.1093/mnras/stu1944/-/DC1)

Please note: Oxford University Press are not responsible for the content or functionality of any supporting materials supplied by the authors. Any queries (other than missing material) should be directed to the corresponding author for the article.

This paper has been typeset from a TEX/LATEX file prepared by the author.